Applied Energy 371 (2024) 123624

Contents lists available at ScienceDirect

Applied Energy

journal homepage: www.elsevier.com/locate/apenergy

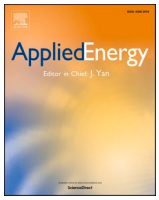

Renewable energy powered membrane technology: Power control management for enhanced photovoltaic-membrane system performance across multiple solar days

Emmanuel Ogunniyi, Bryce S. Richards *

Institute of Microstructure Technology (IMT), Karlsruhe Institute of Technology, Hermann-von-Helmholtz-Platz 1, 76344 Eggenstein-Leopoldshafen, Germany

HIGHLIGHTS

- Optimise daily energy use of photovoltaic-powered membrane desalination system
- Control algorithms: Directly-coupled & Semi-active, with & w/o supercapacitors (SC)
- ~1000 L per day produced during 3–7 day tests performed under different solar days
- Control system with SC afforded: 1) 6–18% lower specific energy consumption (SEC);
- 2) 42–83% improved water quality; 3) the highest (99.6%) load-matching efficiency

GRAPHICAL ABSTRACT

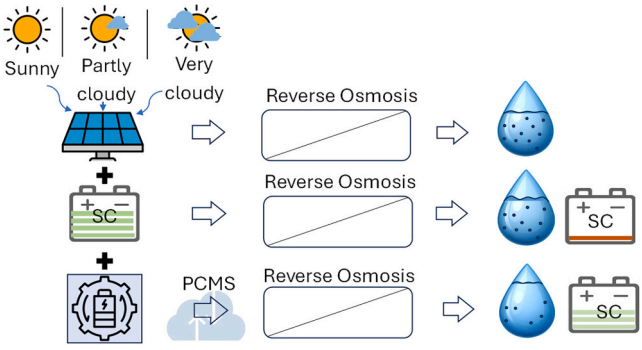

ARTICLE INFO

Keywords:
Desalination
Power control management system
Photovoltaic
Programmable logic controller
Reverse osmosis
Semi-active topology

ABSTRACT

In a directly-coupled photovoltaic-powered membrane desalination (PV-membrane) system, the solar power supply must exceed a certain threshold for the pump to generate sufficient hydraulic pressure to overcome the membrane's osmotic barrier. Below this threshold, no appreciable membrane flux is produced, meaning PV power is underutilised or dissipated by the system. In this work, a power control management system (PCMS) is designed to harvest the underutilised PV power into a supercapacitor (SC) to, firstly, buffer the periods of solar irradiance fluctuations during daily operation. Secondly, this also fosters a continuous stable operation of the PV-membrane system across multiple solar days. The investigation compared the performance of the PCMS against two other configurations: "directly-coupled" (passive, no SC) and "semi-active" (with SC, but no PCMS). During a three-day test desalinating brackish water (5 g/L salinity), the PCMS enabled an improvement in water quality, with the permeate electrical conductivity (EC) 46% and 23% lower than the other configurations, respectively. The specific energy consumption (SEC) was reduced by 18% and 6%, respectively, during the same period. During a week-long experiment, the PCMS facilitated the production of 6218 L of potable water at an average EC of 0.52 mS/cm, while maintaining a minimum state-of-charge of the SCs to about 40%, allowing for subsequent use. The system also achieved a maximum load-matching efficiency of 99.6%, surpassing the 94.7%–96.6% observed in the other configurations. These results pave the way for maximising daily PV energy utilisation,

* Corresponding author.
E-mail address: bryce.richards@kit.edu (B.S. Richards).

https://doi.org/10.1016/j.apenergy.2024.123624
Received 20 December 2023; Received in revised form 25 April 2024; Accepted 1 June 2024
Available online 17 June 2024

ensuring steady and dependable clean water production for the community and improving the water-energy nexus.

Nomenclature

Special characters

€	Euro
g	acceleration due to gravity, 9.81 m/s
Φ	load-matching factor
π	osmotic pressure (bar)
R	ideal gas constant in L·bar/(mol·K)
ρ	liquid density, kg/m3
$	US dollar

Symbols

Imp	current at maximum power point.
IPV	photovoltaic current
ISC	supercapacitor current
Pmp	power at maximum power point
PPump_ref	pump power threshold reference
PPV	photovoltaic power
PPVmin	minimum photovoltaic power to produce flux
Vmp	voltage at maximum power point
VPV	photovoltaic voltage
VSC	supercapacitor voltage
VSCmin	supercapacitor minimum cut-off voltage
VSCmax	supercapacitor full charge voltage

Abbreviations

DC	direct current
DoD	depth-of-discharge
EC	electrical conductivity
ESS	energy storage system
GUI	graphical user interface
HMI	human-machine interface
KIT	Karlsruhe Institute of Technology
LCOW	levelized cost of water
LCOE	levelized cost of electricity
MPPT	maximum power point tracker
PCMS	power control management system
PLC	programmable logic controller
PV	photovoltaics
RO	reverse osmosis
SAS	solar array simulator
SC	supercapacitor
SCADA	supervisory control and data acquisition
SDGs	sustainable development goals
SEC	specific energy consumption
SI	solar irradiance
SoC	state of charge
SSRs	solid-state relays
STC	standard test conditions
TDS	total dissolved solids
TMP	transmembrane pressure
UF	ultrafiltration
UN	United Nations
WHO	World Health Organization

1. Introduction

1.1. Motivation

Water security – society's capacity to have sufficient quality freshwater for survival and to carry out a range of productive activities – is being threatened at various places in the world (particularly in lower latitude and subtropical regions [1]) due to climate change [2]. One way to address this is to no longer rely on fresh surface water, but instead by desalinating brackish water – a naturally occurring water source found underground that is readily available in many regions of the world, albeit with varying quality [3]. With an appropriate desalination method, a relatively high total dissolved solids (TDS) content in brackish water (1–10 g/L) [3,4], is brought close to that of freshwater, typically containing TDS $\leq$ 0.6 g/L [5–9]. According to the World Health Organization (WHO), water with such low TDS levels is generally deemed palatable for drinking purposes [9]. Since energy is an important requirement for desalination [10], the use of green electricity – for example, from photovoltaics (PV) – could contribute an additional benefit in reducing greenhouse gas emissions and mitigating climate change.

Photovoltaic-powered membrane desalination (PV-membrane) system represents one example of a renewable-energy powered water desalination technology, where a high-pressure pump could be driven directly by PV power (directly-coupled), or with the inclusion of an energy storage option (semi-active topology). Small-scale, decentralized, PV-membrane systems can play an important role for the provision of clean drinking water in rural areas of both developed and developing countries [11], where water and electrical infrastructure is often lacking. The degree to which solar power as utilised in a PV-membrane system is mostly influenced by the quality of load-matching [12,13], while the membrane system performance is limited by the amount of solar irradiance (SI) which can be prone to fluctuations and intermittency [14–18]. The load-matching factor ∅ represents the ratio of the actual power consumed by the load (P_{load}), to the measured power generated by the PV array (P_{pv}), as given in Eq. 1. The ∅ can also be formulated in terms of energy, thus indicating the amount of daily PV energy that is utilised by the system [12,13]:

$$\varnothing = \frac{P_{load}}{P_{pv}}. \quad (1)$$

The quality of load-matching for different PV-powered loads has been investigated [12,19–22]. Applebaum [12] demonstrated that the operation of the load-line is always close to the PV power ($P_{load} \approx P_{pv}$) in a perfectly matched system. A discrepancy occurs when the PV supply is above the maximum power demand threshold of the load ($P_{load} < P_{pv}$). In a PV-powered water pumping system, the main electrical load is the pump, which has the hydraulic characteristics of pump head H (m) and the liquid flow rate Q (m^3/s) [23–25]. The maximum hydraulic power P_{hyd} (W) and the feed pressure p (bar) developed by the pump are related by the following expressions [26]:

$$P_{hyd} = p.Q.k\,, \quad (2)$$

$$p = \rho.g.H \approx 0.981\ H \quad (3)$$

k is the pump's efficiency constant, ρ is the liquid density, kg/m^3 (1000 kg/m^3 for water), and g is the acceleration due to gravity, 9.81 m/s^2. Further reports [27–31] have emphasized Ø as crucial for optimising

the performance of a PV-powered water pumping system. This involves aligning the power output of the solar panels with the pump head which could, for example, be achieved via a control algorithm or maximum power point tracker, to ensure maximum energy utilisation. To improve load-matching, an additional electrical load could be activated in parallel with the pump when $P_{pump} < P_{pv}$ or the excess energy stored in energy storage backup to be used or fed back into the grid [28,32,33].

1.2. Solar irradiance fluctuations and control

Fluctuations in SI lead to PV power supply ramping in PV-membrane systems [17]. During ramp-down events, the P_{hyd} of the pump could fall below the membrane osmotic barrier. To compensate for this, the pump necessitates prolonged operational periods to achieve requisite production levels, concurrently intensifying efforts to sustain the essential pressure. Consequently, this leads to an increase in the SEC. The other direct effects of SI fluctuations on PV-membrane system performance include a reduction in flux and permeate quality [17,34–36], expressed in terms of EC.

A large number of system shutdown events (85 per day) were reported by Li et al. [17] during a very cloudy solar day that exhibited rapid fluctuations (voltage ramp rate of ≥2 V/s). The other effects of SI fluctuations on the performance of directly-coupled PV-membrane systems – measured in terms of SEC, flux and the permeate EC, have been reported in other research works [14,15,18,37,38]. For example, Richards et al. [14] demonstrated that SI levels within the range of 400–1200 Wm^{-2} can produce respectable flux (>5 $L/m^2/h$) in a directly-coupled PV-membrane system equipped with a reverse osmosis (RO) element (BW30, Dow Filmtec) for the desalination of brackish water (5 g/L dissolved salt). Below the SI of 300 W/m^2, the ramp-down event produced little or no flux (≤ 1 $L/m^2/h$). Li et al. [15] compared the performance of a directly-coupled PV-membrane to a PV/battery steady-state operation using a 2.4 kWh lithium-ion (Li-ion) battery. The report shows that a directly-coupled system has an increased SEC (~3% sunny day; 15% very cloudy day) and reduced flux (12% sunny day and 39% very cloudy day). Turki *et.al* [18] report that an autonomous directly-coupled PV-membrane remains a challenge, with the difficulty being the ability to effectively manage the fluctuating PV power supply to maximise production. The analysis of RO operation powered by variable PV power [35] emphasized the need to vary the operating level of a RO system to improve the PV-membrane load matching while operating at variable PV power. Additionally, an energy storage backup system in the case studies was found to have enabled a more cost-effective operation as compared to the systems with no backup.

RO membranes are recommended to operate under steady-state conditions [39], thus the effects of SI fluctuating should be minimised to improve the overall system performance [18,40,41]. To address this, two approaches have been pursued: i) oversizing of the PV array [42] and/or ii) adoption of energy storage options [43–45]. The expansion of PV array would necessitate the inclusion of additional power electronics converters and/or direct current (DC) inverter which could contribute to the additional increase in system design cost contingency [42]. Energy storage options are used for maintaining a regulated DC power supply and for storing the (excess) PV energy which can later be released on demand [43–45]. Batteries and supercapacitors (SC) are usually used for this purpose as they can be properly sized to directly support the load demands during the periods of low, fluctuating and intermittent SI [43]. Since the SCs are characterised by fast charge and discharge rates, they are suitable for DC bus stabilisation and peak power supply to the load, while batteries are usually prioritized for high energy demand applications [46]. The power and energy densities of a SC (100–10,000 W/kg; 0.1–15 Wh/kg) and battery (Li-ion = 340–1000 W/kg; 90–260 Wh/kg) can complement each other in various applications when used together. With appropriate DC coupling topology, these features can be utilised to improve the power stability in DC-powered systems [47,48].

1.3. Battery/SC DC coupling topologies

The battery/SC coupling topologies represent different methods of configurations by which the energy storage system (ESS) element can be controlled and cycled to drive a DC system. The three common coupling topologies are passive (directly-coupled), semi-active and fully-active, which have been extensively researched [49–54] and are summarised in Fig. 1.

In the passive configuration (Fig. 1a), the ESS is directly connected in parallel across the load. The DC current sharing is largely determined by the respective internal resistances of the ESS without a control system [50, 55]. In parallel fully-active, Fig. 1b-d, the outputs from both DC/DC converters are connected in parallel to the DC bus and controlled with various energy management algorithms to regulate the DC bus voltage output. Figs. 1e-f represent the semi-active configurations where one bi-directional DC/DC converter is used to decouple the battery and/or SC and control the DC bus. The diode hybrid (Fig. 1g) meanwhile has the tendency to operate in passive or semi-active mode via a unidirectional DC converter. In systems where more than two ESS are hybridised, a multi-level hybrid ESS configuration (Fig. 1h) allows flexibility in power sharing among the ESS with or without DC/DC converters [54].

1.4. Semi-active topology

The most commonly adopted topology is semi-active, where one energy storage device (e.g., the SC) is connected directly to the load and the other (e.g., the battery) is controlled for charging and discharging via a bi-directional DC/DC converter, as illustrated in Fig. 1e-f. The method can offer improved system efficiency when the SC responds to buffer the rapid and/or successive power fluctuations in the DC power supply [51–54]. For example, the performance of battery/SC semi-active topology in a hybrid electric bus was reported by Min et al. [52]. Over a drive range of 23.2 km (~43 mins), this enabled a fuel consumption saving of 7% compared to battery-only powered over the same range [52]. Ibanez et al. [51] simulated passive and semi-active topologies and compared the results to a battery-only powered electric motorcycle (5 kW motor). The results show that the total energy supply from the battery (Li-ion 24 V, 50 Ah, 1.2 kWh) and SC (0.018 kWh) in semi-active topology increased by 6.6%. Due to the limited efficiency of the DC/DC converter, the actual energy delivered to the load was reduced to 3.0%.

By simulating the performance of a 50 W PV panel (V_{mp} = 17.5 V, I_{mp} = 2.9 A, 25 °C, SI =800 W/m^2), a valve-regulated lead-acid battery (12 V 17.2 Ah, 0.206 kWh) and SC bank (12 V 1200 F, 0.024 kWh), Glavin et al. [53] indicated the performance of semi-active topology equipped with bi-directional DC/DC converter for different load current peaks. The report shows that the addition of a SC bank in the energy management system reduced the discharge stress on battery during operations. The battery state of charge (SoC) increased by 12% for peak load and 11% for pulsating current loads while there was a reduction of battery SoC by 3% under constant current load. For a stand-alone rural electrification system, Jing et al. [54] also demonstrated by simulation that the combination of PV power with battery and SC in semi-active topology can minimise the depth-of-discharge (DoD) of the respective storage units.

Largely, when battery/SC is properly controlled with respect to the load demand and the available PV power supply, the peak current demand and discharge stress on the storage units can be minimised [56,57]. Additionally, a controlled semi-active topology can improve the utilisation of PV power as well as the quality of daily load matching [12]. To improve the overall system performance, the semi-active topology is expected to be realised with the minimum number of power conversion units (e.g., DC/DC converter), as these would reduce additional power loss due to the limited efficiency converter's [55].

In PV-membrane systems, the controlled semi-active topology has received little attention, especially for sustaining resilient autonomous operation. The aforementioned prior empirical investigations have

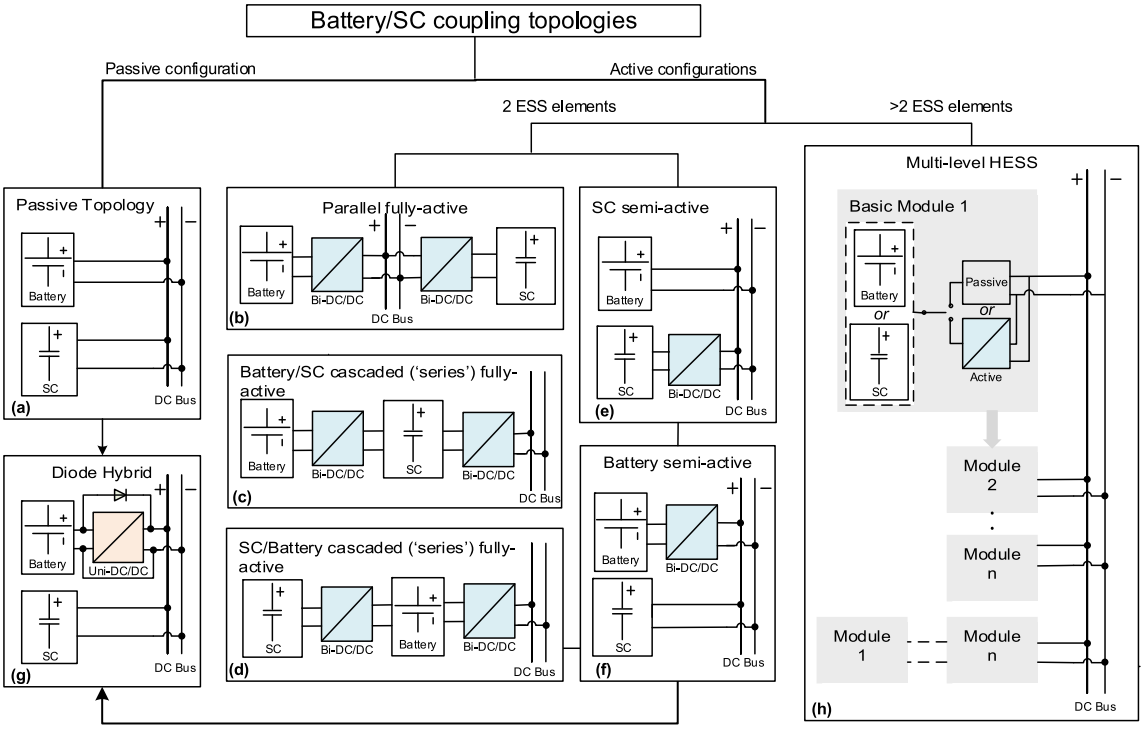

Fig. 1. Overview of battery/SC topologies: (a) passive; (b) parallel fully-active; (c) battery/SC cascaded fully-active; (d) SC/battery cascaded fully-active I SC semi-active; (f) battery semi-active; (g) diode hybrid semi-active; (h) multi-level hybrid ESS. (bi-DC/DC = bi-directional DC converter; uni-DC/DC = unidirectional DC converter).

mostly focused on the directly-coupled operation and uncontrolled battery/SC coupling for short time (minutes to few hours) energy buffering [14–18,37,38,58].

When a PV-membrane system directly-coupled, and the power generated by the PV is less than the minimum threshold demand by the pump to generate sufficient hydraulic pressure to produce significant flux (permeate) across the membrane, the PV energy is inefficiently utilised for production. It dissipates within the system primarily to meet the operational demands of the pump [59,60]. When battery/SC is incorporated without the possibility of controlled synchronous charging during daily operation, the charge capacity becomes depleted after a short duration (minutes to hours) [61,62]. Thus, a continuous autonomous operation supported by storage cannot be sustained across multiple solar days.

A controlled semi-active topology is significant for enabling an effective power control management system (PCMS) in a PV-membrane unit. A PCMS refers to a system that monitors and regulates the use of power within a particular system. It typically consists of sensors, controllers, algorithms, and monitoring devices, designed to gather data, control, and optimise power consumption, distribution, and storage [63–65]. Notably, the investigation of controlled semi-active topology to maximise the daily utilisation of PV power supply for PV-membrane systems is still limited. When a controlled semi-active topology is effectively implemented for a PV-membrane system, this could significantly optimise the PV power utilisation and effectively manage the charging cycles of energy storage units, thereby enhancing overall system performance across different solar days.

1.5. Research questions

This work focuses on the development and implementation of a controlled semi-active topology to establish an effective PCMS within a PV-membrane system. The primary aim was to optimise the utilisation of daily PV power to sustain continuous autonomous operation spanning multiple days under varying SI conditions. To address this objective, the following research questions were investigated:

- PV-membrane system performance with semi-active topology: How does a PV-membrane system performance – in terms of load-matching, flux, SEC, EC – differ when employing a semi-active topology compared to directly-coupled operation, and how effective is the semi-active approach for an autonomous PV-membrane operation?
- Energy storage sustainability for daily operation using controlled semi-active topology: In an autonomous PV-membrane operation where daily synchronous recharge of the energy storage unit is not feasible, to what degree does a controlled semi-active topology contribute to sustaining daily autonomous operation, particularly regarding the durability of the energy storage?
- PCMS for multiple days operation: How does the integration of a controlled semi-active topology enable an effective PCMS to sustain continuous autonomous operations over multiple days amidst fluctuating and intermittent SI conditions?

Addressing these inquiries could lead to enhanced system performance, characterised by improved load-matching, increased daily production, and achieving acceptable drinking water quality with low SEC across various solar days. Furthermore, the investigation would provide insights into strategies to bolster system reliability and develop efficient power control management methodologies, enabling sustained and efficient energy utilisation for continuous multi-day operations.

2. Materials and methods

In the development of a PCMS requiring frequent energy storage cycling, SCs stands out for their exceptional cycling capability, surpassing conventional batteries with up to 1 million charge-discharge cycles being possible. Typically, the energy density of SCs is low (0.1–15 Wh/kg), however, more recently, higher energy density SC modules have been developed. When a SC achieves a high energy density – comparable to that of a Li-ion battery – it becomes a preferable alternative within such PCMS. Leveraging this advantage, a high-

energy-density SC module is integrated into the developed PCMS in this work, replacing the conventional Li-ion battery. This strategically combines the beneficial characteristics of both the battery and SC, thereby contributing to the enhancement of the overall performance of the PV-membrane system. Additional details regarding the system setup are presented in this section.

2.1. PV-membrane system

The schematic of the PV-membrane system used in this study is shown in Fig. 2. The main system components of the setup include the ultrafiltration (UF) membrane for pre-treatment coupled with a RO membrane for desalination; the PV array, the output power characteristics of which were emulated in using a solar array simulator (SAS); charge controller, SC module, DC pump and a programmable logic controller (PLC).

The PV power can be supplied directly by the PV panels or emulated via the SAS. The PV supply is connected via a charge controller to the SC module. The pump can then be powered by the SC module or directly from the PV supply with respect to the control algorithm executed by the PLC. The sensors in the system are current and voltage sensors, pressure sensors, flow rate sensors, and EC sensors. Each sensor outputs an analogue signal (4–20 mA), which is transmitted to the PLC for subsequent processing and control, discussed further in Section 2.1.6.

In the following sub-sections, the specifications of the main system units, components, and devices are presented, while further details regarding the characteristics and modes of operation of the sensors and devices are provided in Tables S5 and S6.

2.1.1. PV panel/SAS:

A solar array simulator (SAS, Chroma 62050H—600S) is used in the laboratory to replicate specific solar days based on collected SI data (detailed further in section 2.1.7). This is to enable a reproducibility of various past solar days or SI conditions for experimental purposes. The SAS, based on a 5 kW-rated DC power supply [66], is programmed to simulate the performance of six PV panels (OffGridTec PCB-ETFE, each panel possessing P_{mp} = 100 W, V_{mp} = 39.6 V, and I_{mp} = 2.53 A, temperature coefficient factor $\beta = -0.45\%/^{o}C$, surface area 0.575 m^2), connected in three series and two parallel configuration to achieve collective maximum values of P_{mp} = 600 W, V_{mp} = 118.8 V, and I_{mp} = 5.06 A. The P_{mp} represent the maximum attainable power under standard test conditions (STC) of 1000 W/m^2 intensity of the air-mass 1.5 global solar spectrum at 25 °C operating temperature. The V_{mp} and I_{mp} are the voltage and current at maximum power under the same STCs. The arrangement is tailored to ensure compatibility between the total V_{mp} of the PV panels and the maximum rated voltage (150 V) of the employed maximum power point tracker (MPPT) charge controller.

2.1.2. MPPT Charge controller:

An MPPT charge controller (Victron Energy SmartSolar MPPT 150 V 70 A) was used in this system. By constantly monitoring the voltage and current of PV panels, an MPPT technology ensures that the available power from the PV is maximally utilised or stored in the storage unit – e.g. battery or SC. The selection of this model was based on its compatibility with PV panels having a V_{mp} of up to 150 V, aligning with the system's PV setup where V_{mp} is 118.8 V. Furthermore, the charge controller is designed to efficiently charge a 48 V-rated battery with a maximum conversion efficiency of 98%. Although a 48 V-rated SC module was used in the system, the MPPT charge controller is also compatible for charging it, given that the terminal electrical characteristics of the SC align closely with those of a 48 V-rated battery.

2.1.3. Supercapacitor:

A 48 V-rated SC module (Sirius, KLW28048, KilowattLabs, United Arab Emirates) is employed, which boasts an extensive cycle life, capable of enduring up to 1 million cycles, and exhibits a high DC energy capacity of 2500 Wh (weight 58 kg). These characteristics provided the advantages, influencing the selection of the SC over the utilisation of a conventional battery within the system as outlined in the introduction of Section 2. Further review on the technological advantages and comparative analysis of SC and other energy storage technologies have been reviewed in other studies [15,45,55,67]. Since the terminal characteristics of this SC module closely align to that of a 48 V battery, it is charged by the MPPT charge controller while the charge-discharge control is intelligently managed by the MPPT charge controller in support with the threshold limits programmed into the PLC control algorithm for experimental operations.

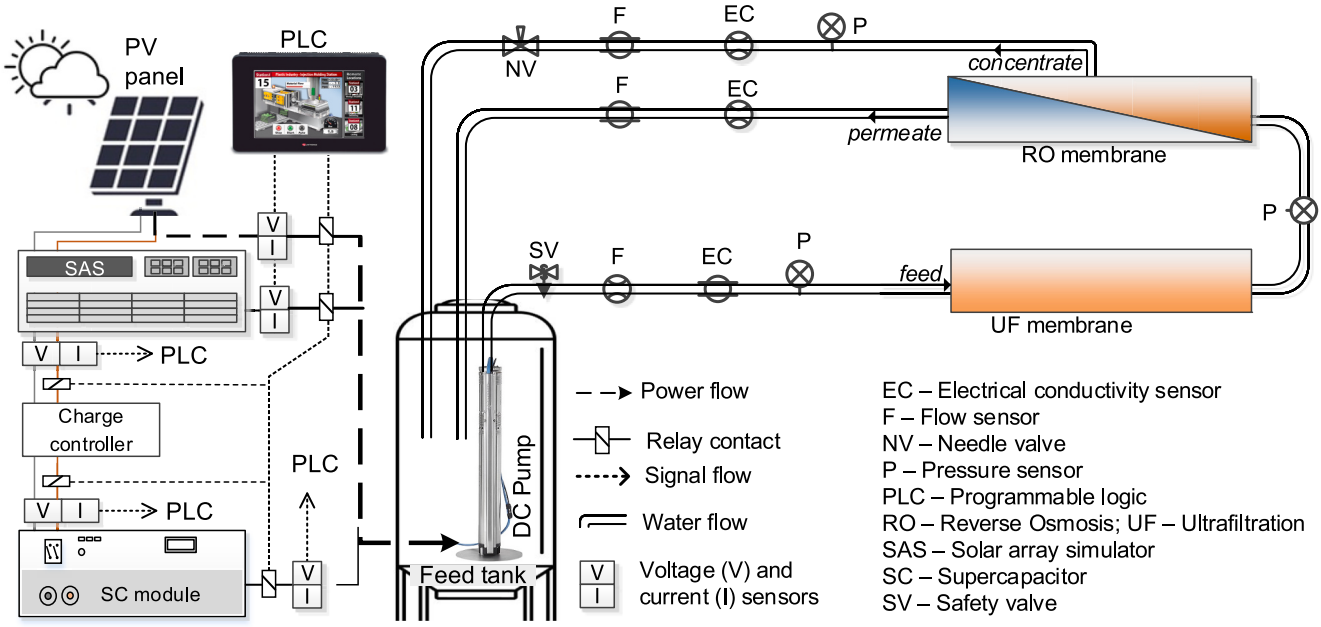

Fig. 2. Schematic of PV-powered membrane desalination system, integrated with PCMS consisting of a SC module, charge controller, PV power supply, DC pump- all controlled and switched via the PLC.

2.1.4. Pump:

A DC helical rotor pump (Grundfos SQFlex 0.6–2 N) is used for the experiments. This exhibits a maximum pump head of 120 m (maximum pressure of 12 bar) and a maximum feed flow rate of 9.8 L/min when driven at 420 W. The pump was selected based on its: i) compatibility with the PV-membrane system to supply the required hydraulic conditions – high pressure and low flow; ii) tolerance for a wide range of salt concentration. The pump's power demand (P) at any time during operation is related to the feed pressure p (bar), feed flow rate Q (L/h), and the pump's efficiency (η) by the following expressions in Eq. 4 [68]:

$$\mathrm{P\ (W)} = \frac{\mathrm{Q\ (L/h)} \bullet \mathrm{H\ (m)}}{367 \bullet \eta}, \tag{4}$$

where H = pump head (m) and η = pump's "wire-to-water" efficiency. The performance characteristics of the pump under the test conditions (water temperature 20 °C, density 998 g/L, pump head of 120 m) are given in the **Fig. S1.**

2.1.5. Membranes, feedwater and recirculation:

Two spiral-wound membranes are used: a pre-treatment stage for removing possible macromolecules suspended in water is realised via an UF membrane (DuPont Dizzer P4040, 6.0 m^2), while desalination is achieved via a low-pressure RO membrane (DuPont FilmTec BW30–4040, 7.2 m^2). Synthetic brackish water – realised by dissolving 5 g/L sodium chloride in de-ionised water (osmotic pressure of 2.09 bar at 20 °C, calculated in section S1.3) – is used for all experiments in this work. The feedwater is stored in a 270 L double-walled tank that facilitates the temperature control of the feedwater to 20.5 ± 0.5 °C. Temperature control is facilitated by a water circulation chiller (Julabo FC600) interconnected with the tank's interlayer wall.

The concentrate (brine) and permeate (fresh water) streams are recycled back into the feed tank to maintain the same feed tank water volume and concentration over long-term experiments. This study however did not consider directly recirculating the concentrate stream solely into the feed tank to increase recovery. This approach could elevate the salinity level of the feed water, potentially compromising the reliability of the experimental results for the investigated topologies. Typically, recirculation of the concentrate stream for higher recovery is achieved through a double pass RO setup, where the discharged concentrate from the primary RO unit is directed to the secondary RO unit. Nevertheless, a significant challenge emerges as the discharge from the primary unit contains elevated concentrations of scaling compounds such as silica and calcium, rendering it unsuitable for direct feeding to the secondary unit without additional pre-treatment to prevent membrane fouling. Additionally, the pump must possess sufficient capacity to overcome the TMP of both RO membranes, presenting operational and economic challenges to the process.

2.1.6. PLC, sensors and signal control:

A PLC (Unistream 10.4″, Unitronics, Israel) is programmed to control the switching operation of the DC power supply from the PV and the energy storage units for driving the system (pump). The analogue signals (4–20 mA) from 17 sensors are fed into the analogue inputs of the PLC: Pressure transmitters (Bürkert 831, 3 units), EC sensors (Bürkert 8222, 1 unit, GF Signet 2822, 2 units), flow sensors (Bürkert 8030, 2 units and Kobold MIM-12, 1 unit), DC current transducers (Phoenix contact MCR-S10–50-UI-SW-DCI-NC, 5 units), and uni−/bipolar DC voltage transmitters (Omega Engineering, DRST-CM 300 VDC, 5 units). These signals are converted into digital values and processed by the PLC's central processing unit. The conversion process involves sampling the analogue signals at regular intervals (1 s) while the converted data is processed according to the controlled algorithm programmed into the PLC's memory. Further information about the sensors is presented in the supplementary information Table S4. After the data is processed by the PLC, control digital signals (on/off) can be generated to control the solid-state relays (SSRs).

The selection of a PLC for integration within the system is predicated upon the key factors such as its high reliability for real-time control, deterministic execution of process commands, potential for system automation and remote accessibility, flexible graphical programming language (ladder logic) and customisable human-machine interface (HMI), which may not be entirely realised with microcontrollers or alternative data acquisition hardware solutions. The user-interactive HMI facilitates the control, monitoring, and process operation by human operators, which distinguishes it from graphical user interface (GUI) devices where the user interface only allows interaction with software applications on systems, computers, or electronic devices. The PLC HMI is additionally relevant for specific machines or subsystems and primarily interact with data from local sensors and control points. Thus, a centralised control system as supervisory control and data acquisition (SCADA) – designed to oversee extensive industrial processes or facilities, specialized for large-scale data acquisition from distributed sensors and devices across multiple sites, may not be applicable to the single unit PV-membrane system in this study.

2.1.7. Solar irradiance information:

The SI data of three solar days – "sunny day", "partly cloudy" and "very cloudy" days – are used for the experiments. This data was selected from one year (2016) of solar data that was measured at the KIT Solar Park in Karlsruhe, Germany (Latitude: 49.0935° N Longitude: 8.4365° E), under high temporal resolution (1 s): i) a sunny day (5 May 2016) with no-clouds; ii) a partly-cloudy day (26 May 2016), which exhibits a series of passing heavy clouds during the middle of the day; and iii) a very-cloudy day (13 October 2016), which serves as a near worst-case scenario in this work. The SI as a function time for these three days – along with the measured rear-side temperature of the silicon PV modules – are plotted in Figs. S2A and S2B. Additionally, to assess the adaptability of the proposed topology under varying conditions, the SI data from three additional solar days were incorporated into a week-long dataset. These additional days encompass: a mostly sunny day (20 June 2016), another mostly sunny day (6 October 2016), and a clear sunny day (18 March 2016). These are furthermore plotted in **Figs. S3A and S3B.**

2.2. Investigated DC coupling topologies and parameters for PV-membrane system

2.2.1. Steady-state tests

To operate PV-membrane system at its system-specific optimal operating condition, it is important to determine the operating threshold at which the system's set point remains fixed for all experiments. This is achieved through steady-state performance tests conducted across various pump demand thresholds. The back-pressure valve is adjusted iteratively at fixed PV power supply to realise different pump's power demand thresholds. The aim is to identify the power demand threshold at which appreciable flux of drinkable quality at relatively low SEC can be realised. This is further reported in section 3.1.

Three direct current (DC) power coupling topologies for the PV-membrane system are investigated, namely: i) directly-coupled (passive); ii) semi-active topology (without PCMS); and iii) adaptive topology with integrated PCMS.

2.2.2. Directly-coupled system (passive topology):

In this arrangement (also referred to as passive topology), a suitably sized PV array, simulated using the SAS, is directly linked to power the pump without additional energy storage provisions or a DC/DC converter. Usually in this configuration, the performance of the PV-membrane system aligns with the peak power trajectory of solar radiation until the generated PV power (P_{PV}) exceeds the hydraulic threshold of the pump. Moreover, the system is susceptible to SI fluctuations, and occasional intermittent shutdowns when the P_{PV} is too low. These

fluctuations may impact water quality and contribute to an increase in SEC [18,40]. This configuration is mostly adopted due to its simplicity and robustness. Illustrated in Fig. 3a, this topology serves as a benchmark reference configuration for assessing the effectiveness of the other two proposed system topologies.

2.2.3. Semi-active topology without PCMS:

This topology shares similarities in configuration with the semi-active topology depicted in Fig. 1e, however modified with a substitution of the battery with a PV power source and replacing the bi-directional DC/DC converter with the MPPT charge controller. Notably, this arrangement provides a distinctive operational advantage, enabling the system to function in a semi-active topology mode without the need for a bidirectional DC/DC converter or additional control algorithms. The determination of charging or discharging states for the SC is intelligently managed by the MPPT charge controller. In this topology (Fig. 3b), the pump and SC are arranged in parallel, drawing from the maximum power supply generated by the PV panel. During instances when PV power exceeds the pump demand threshold (typically around solar noon or peak periods), the discharge rate of the SC markedly diminishes, with the pump predominantly reliant on the PV power supply. Conversely, when the PV power falls below the pump demand threshold, the SC supplements the required power demand for the pump.

2.2.4. Semi-active topology with PCMS (adaptive topology):

This proposed configuration enables selective operation of the SC in semi-active mode while providing the flexibility for the system to function in a directly-coupled setup. The control algorithm, (discussed in Section 2.4.2), governs the charging and discharging cycles of the SC module based on varying SI conditions, the pump's demand and the SC SoC. This configuration is adaptive because it systematically mitigates the impact of SI fluctuations on the PV-membrane system's performance across different solar days, while consistently maximising the daily utilisation of PV power supply under different SI conditions. The energy stored in the SC during controlled operations serves to buffer the SI fluctuations in the subsequent day's operation. Illustrated in Fig. 3c, this process allows bidirectional switching facilitated by low-power (10–50 mW) solid-state relays (SSRs) controlled through the PLC, eliminating the need for bidirectional DC/DC converters, whose limited efficiency could further reduce the overall utilisation of PV power supply.

Using the three topologies depicted in Figs. 3a-c, the following PV-membrane performance parameters were investigated under daily continuous operation: a) Electrical parameters: i) PV power supply, ii) pump power demand, iii) SEC, iv) SC charge-discharge variations; b) Water quality and production metrics: i) permeate EC, ii) flux, iii) daily production. For steady-state tests, the following parameters are moreover additionally investigated: i) feed pressure, ii) transmembrane pressure (TMP), iii) rejection, and iv) recovery. These parameters are examined under steady-state conditions because, during continuous operation, they tend to undergo continual variations due to changes in SI conditions, hence better understood at steady-states. Further discussion on each parameter is given in the supplementary information section S1.

2.3. Pump's operating power threshold and setpoint initialisation

The operational power reference threshold for the pump represents the minimum electrical power required to ensure the production of high-quality permeate (EC < 0.5 mS/cm) from a brackish feedwater source during the RO desalination process. This threshold was empirically determined by varying the pump's power demand within the range of 250 W to 450 W. As the supply feed pressure correlates directly with power consumption (Eqs. 2–3), the pump's power demand are established by controlling the flow pressure by manipulating the position of the back-pressure needle valve on the concentrate stream (refer to Fig. 2). The initialization of the power demand setpoints is done through the following experimental processes:

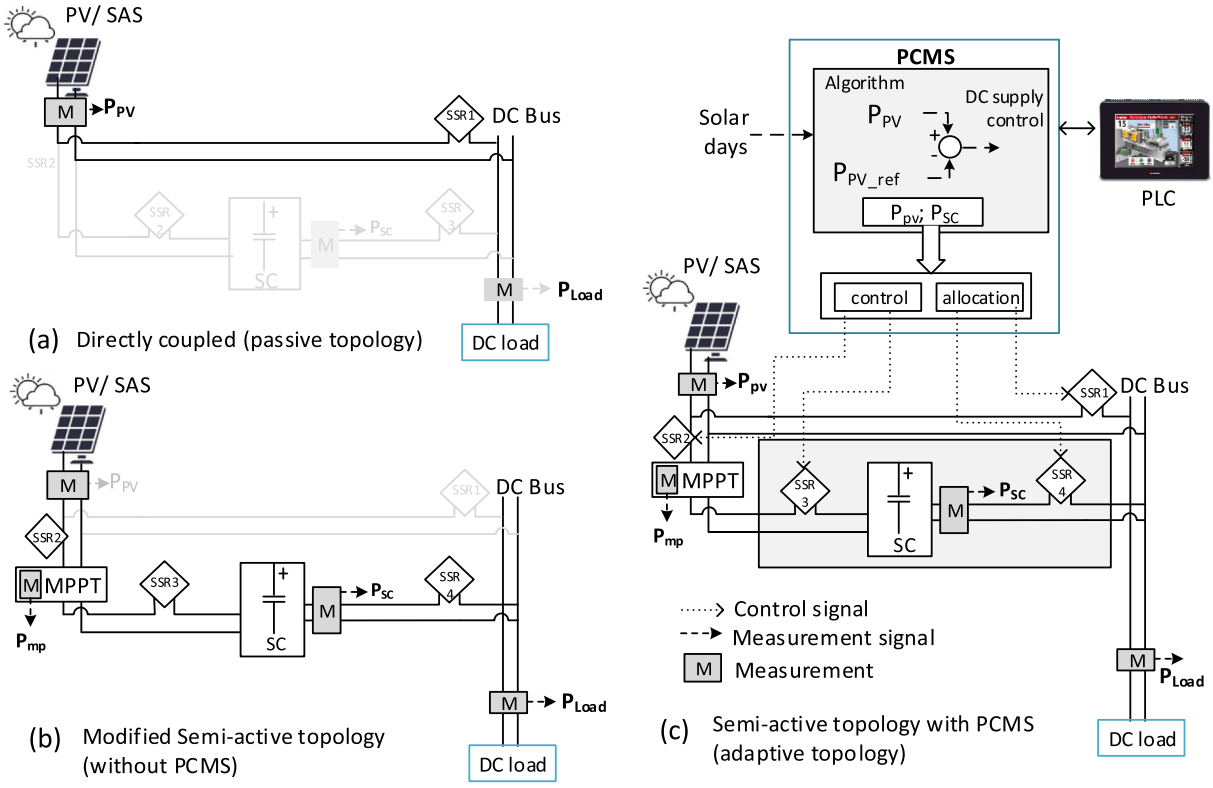

Fig. 3. The three different topologies of the PV/membrane experimentally investigated within this work: **(a)** Directly-coupled (passive topology). **(b)** Semi-active topology (without PCMS) **(c)** Semi-active topology with integrated PCMS (adaptive topology).

i. The SAS is programmed with fixed SI and temperature parameters set at 1000 W/m^2 and 25 °C, respectively. These settings represent the STCs under which the PV panel rating was determined (section 2.1.1). Under these conditions, the PV panels can supply up to a maximum power output of 601 W to the PV-membrane system across varying solar days.
ii. The adjustment of the back-pressure needle valve continues until the specified pump's demand thresholds are achieved. The PLC monitors the pump's power via the output from I-V sensors, as illustrated in Fig. 2. The investigation covers thresholds from 250 W to 450 W at 25 W step intervals, reported in section 3.1.

2.4. Supercapacitor and PV power control strategy

To effectively regulate the DC power coupling from both the SC and PV system to drive the pump, while synchronously recharging the SC from the PV, specific control inputs are necessary. These inputs play a pivotal role in formulating the control algorithm aimed at maximising the utilisation of PV power for the PV-membrane system across various solar days.

2.4.1. SC method of control

The control methodology of the SC relies on the PV power deviation (Eq. 5) and the SoC of the SC, which is characterised by the SC voltage level due to a rough linear correlation between SoC and the voltage of SCs. While the SC's charge level remains within the predefined range, the system operates continuously with the SC providing buffering support throughout the day until either or both the following SC discharge cutoff conditions are met: $V_{SC} = V_{Scmin}$ (46 V), $P_{PV} < P_{PVmin}$ (250 W). The P_{PVmin} is experimentally determined through the steady-state threshold tests (section 3.1). At P_{PVmin}, the available PV power is insufficient to produce an appreciable flux through the membrane. Consequently, when the P_{PV} falls below P_{PVmin}, it is redirected to charge the SC through the SSRs which are switched on/off via the control signals received from the PLC. The control algorithm is implemented in the PLC (Fig. 3c) using ladder logic programming language. At the start of the control process, the PLC senses the signal input from the voltage and current transducers in the system (I_{PV}, V_{PV}, I_{SC}, V_{SC}). These are used to determine the respective relevant PV and SC power references.

2.4.2 PV power control:

The PV power deviation (P_{PV_dev}) signifying the power difference between the instantaneous PV power supply and the pump's demand reference (P_{pump_ref}) – serves as the primary control input in this study as defined in Eq. 5:

$$P_{PV\_dev} = P_{PV} - P_{pump\_ref}, \quad (5)$$

where P_{PV} is the instantaneous PV power, and P_{pump_ref} (350 W, as determined in section 3.1 via steady-state testing), denotes the pump power reference threshold to produce an appreciable flux of drinkable quality at relatively low SEC. As given in Fig. 4, the P_{PV_dev} enables a positive or negative deviation, which is used to trigger various switching states within the control algorithm. The SC moreover here undergoes conditional charging during positive deviation when the PV power supply exceeds the maximum pump demand corresponding to the operating pump head.

3. Results and discussion

3.1. Steady-state tests of the PV-membrane system

To determine the referenced power demand threshold of the pump, steady-state tests were conducted across a range of power demands, spanning from 250 W to 450 W in increments of 25 W as shown in Fig. 5. The PV power limit (P_{PVmin}) of 250 W, as experimentally determined, represents the lower threshold, below which the pump's pressure is inadequate to generate a notable flux. Conversely, 450 W serves as the upper threshold, indicating the extreme operating condition of the

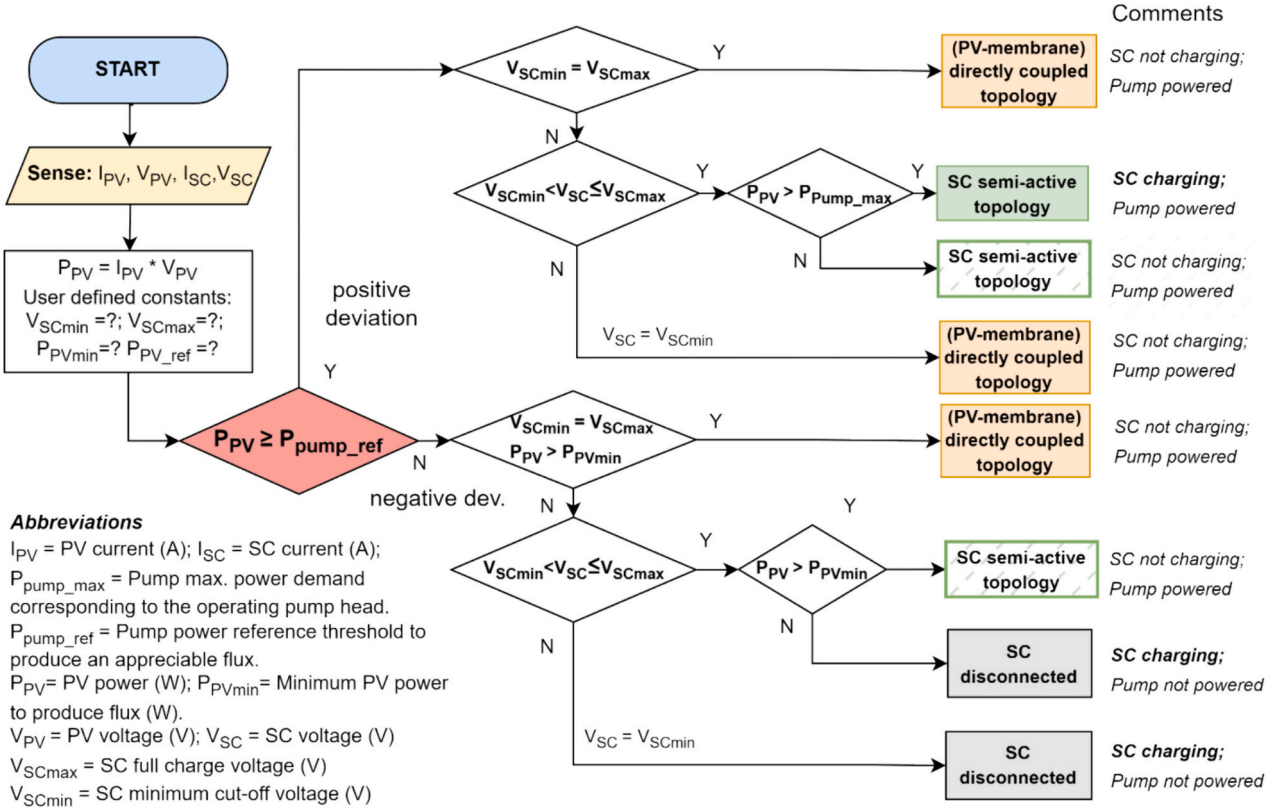

Fig. 4. Adaptive control algorithm for maximising PV power utilisation for PV-membrane system on different solar days.

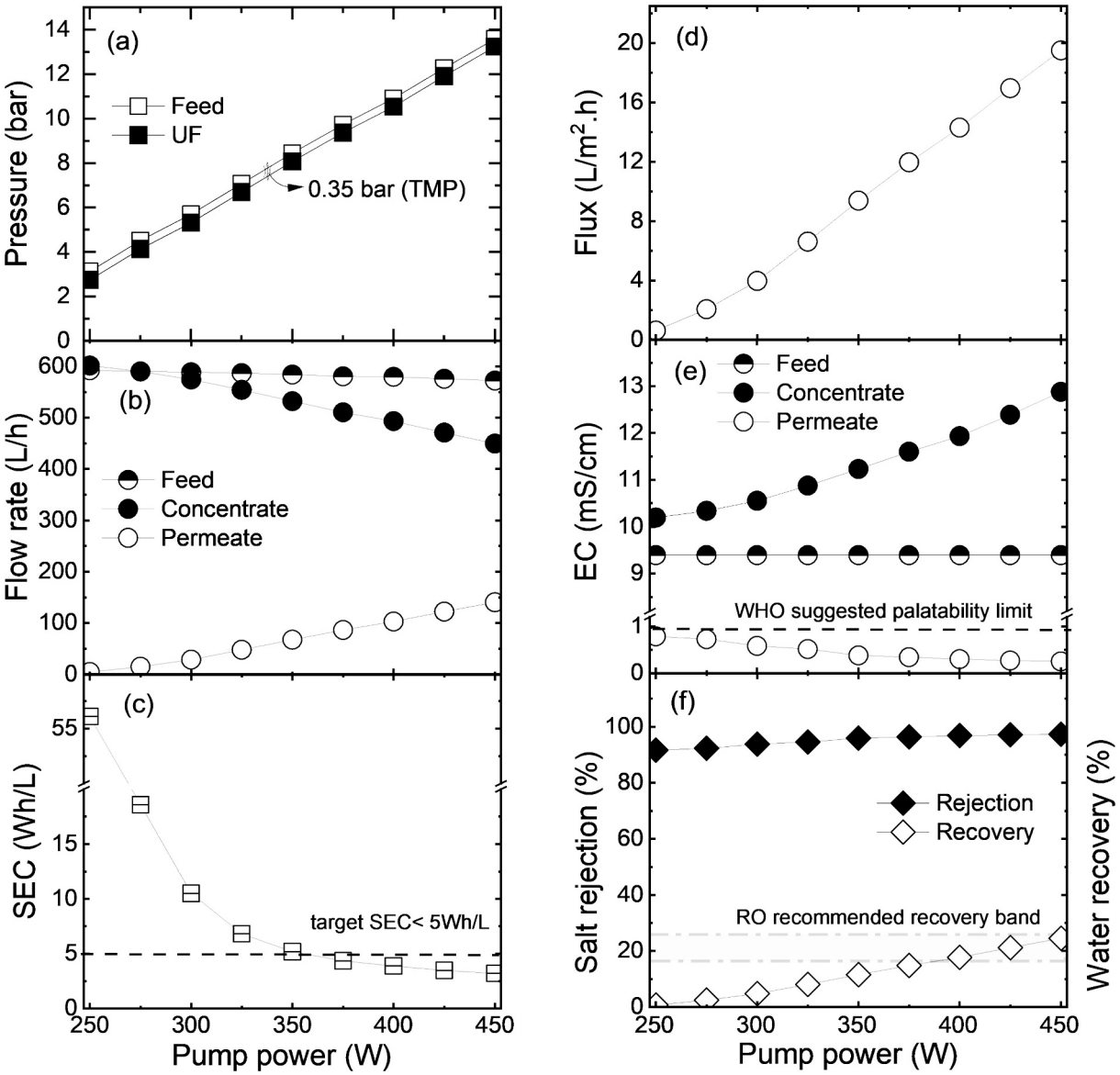

Fig. 5. Steady-state threshold tests of PV-membrane system: (a) Pressure, (b) Flow rate, (c) SEC, (d) Flux, I EC, (f) Salt rejection / Water recovery. The WHO's suggested palatable limit of 0.6 g/L TDS in drinking water [9] is converted to EC and plotted here as 1.133 mS/cm.

pump, slightly surpassing its maximum pump head of 420 W [68]. As the load demand surpasses the maximum pump head, both flux and SEC may momentarily improve during steady-state operation. However, when a pump generates excessive pressure, leading to a high membrane recovery rate surpassing the recommended maximum, it can prompt salt accumulation on the membrane surface, potentially causing scaling in RO membranes. The pump was operated at its maximum pump head, which correspond to a maximum feed pressure of 12 bar, flux of 17 L/m^2.h, and a recovery of 24%. This recovery is consistent with the manufacturer's recommendation recovery of 18–24% for the employed membrane type (BW30–4040) [39]. Thus, the operating recovery of 24% was maintained across all explored topologies. Thus, the operating recovery of 24% was maintained across all explored topologies.

To realise each specified power demand, the back-pressure valve (Section 2.3) was adjusted iteratively, while the pump's power consumption was monitored via the PLC. Upon reaching the desired demand threshold, the system operated in steady-state mode for a duration of 30 min. The following performance indicators were mainly used to evaluate the productivity of the system: Low SEC $<$ 5 Wh/L, permeate EC $<$ 1.133 mS/cm (to maintain drinkable water guideline as given in section 1.1), and recovery ratio in the range of 18–24% (to enable operation within the recommended range where the chance of concentration polarization of the membrane will be minimised. Other parameters of interest include the following: pressure, flow rates, flux, and rejection. The results are presented in Fig. 5, while a summarised overview of the parameters is provided in the supplementary information Table S1.

The rise in the pump power demand corresponds to an increase in the feed pressure, with a consistent TMP of about 0.3 bar (Fig. 5a). The rise in feed pressure causes the permeate flow rate to increase with a corresponding decline in the concentrate flow rate (Fig. 5b) to maintain the mass balance. A low SEC of $\leq$5 Wh/L, which has been mostly reported for brackish water desalination with RO membrane systems, is achieved at a pump power demand of at least 350 W (Fig. 5c). The corresponding flux (permeate flow rate per membrane surface area) is shown in Fig. 5d, while Fig. 5e illustrates changes in water quality measured by reductions in EC values.

Primarily, the TDS concentration in water correlates with the EC level of the solution. The study reported a salinity of 5 g/L, which corresponds to 5 g of NaCl measured and added to 1 L of deionized water at

20 °C. This gave an EC reading of 9.435 mS/cm (or 1 g/L NaCl ≈ 1.887 mS/cm). Considering the possibility of variations in conversion factors in other studies – which could be influenced by experimental conditions, this suggests caution in implementing a returned conversion which may not analytically indicate the precise amount of TDS in the water. Therefore, to ensure methodological consistency, the EC measurements were subsequently used in the study to determine the water quality assessment. The previously cited permissible TDS level in drinking water of 0.6 g/L [9]. This corresponds experimentally to a permeate EC of 1.133 mS/cm, serving as the benchmark for assessing water quality in this study.

The percentage of salt rejection (the efficiency of an RO membrane in removing dissolved salts and other solutes from a feedwater source) and water recovery (the ratio of permeate volume produced to the volume of feedwater) as shown in Fig. 5f, represent other important performance parameters of the PV-membrane system.

The significant threshold conditions for the control algorithm incorporated with the PCMS were determined using the steady-state tests: A pump power of 350 W was identified as the threshold reference (P_{Pump_ref}) where flux can be produced with relatively low SEC < 5 Wh/L. Additionally, the PV power supply of 250 W was used as P_{Pvmin}, as there was no appreciable flux produced below this limit. These set thresholds are pump specific and steady-state tests may be required when using other pump types. In the control process, the discharge/buffering of the SC begins upon the attainment of $P_{PV\_ref} = 350$ W and it terminates when the minimum charge level $V_{Scmin} = 46$ V or when the PV power diminishes below 250 W (P_{Pvmin}) towards day's end. These conditions were maintained across all experimental tests to facilitate comparative analysis. In the supplementary information, **Fig. S5** contains the data pertaining to the steady-state threshold tests, while **Fig. S6** presents the results of daily performance tests conducted at various pump power demand thresholds. The findings relating to the various investigated topologies are detailed in the subsequent sections.

3.2. Directly-coupled topology – Solar days

The directly-coupled PV-membrane system was investigated for continuous operation under three different SI conditions. For three days of operation (days 1–3), Figs. 6a-c show the percentage of daily load-matching and demonstrate how variations in PV power (resulting from the SI fluctuations) can influence the pump's power demand and system shutdowns. Furthermore, the maximum PV power is not fully harnessed once the pump's peak power demand was reached as shown in Figs. 6a & b. The corresponding daily flux produced, and the cumulated daily production are shown in Figs. 6d-f. The PV power fluctuations led to spikes in SEC, and average EC values of the permeate often exceeded the recommended safe drinking thresholds (1 mS/cm) as shown in Figs. 6g-i.

Over the three days of operation, the load-matching ranges between 95.0% and 96.6%. The cumulative production amounted to 2687 L, with an average permeate quality measuring at 0.73 mS/cm and the average SEC of 4.1 Wh/L. The low SEC and high production with this topology were realised by operating the system at highest possible recovery rate at 450 W as earlier determined in Fig. 5.

3.3. Semi-active topology (without PCMS) – Solar days

In an uncontrolled semi-active topology approach, a SC module was

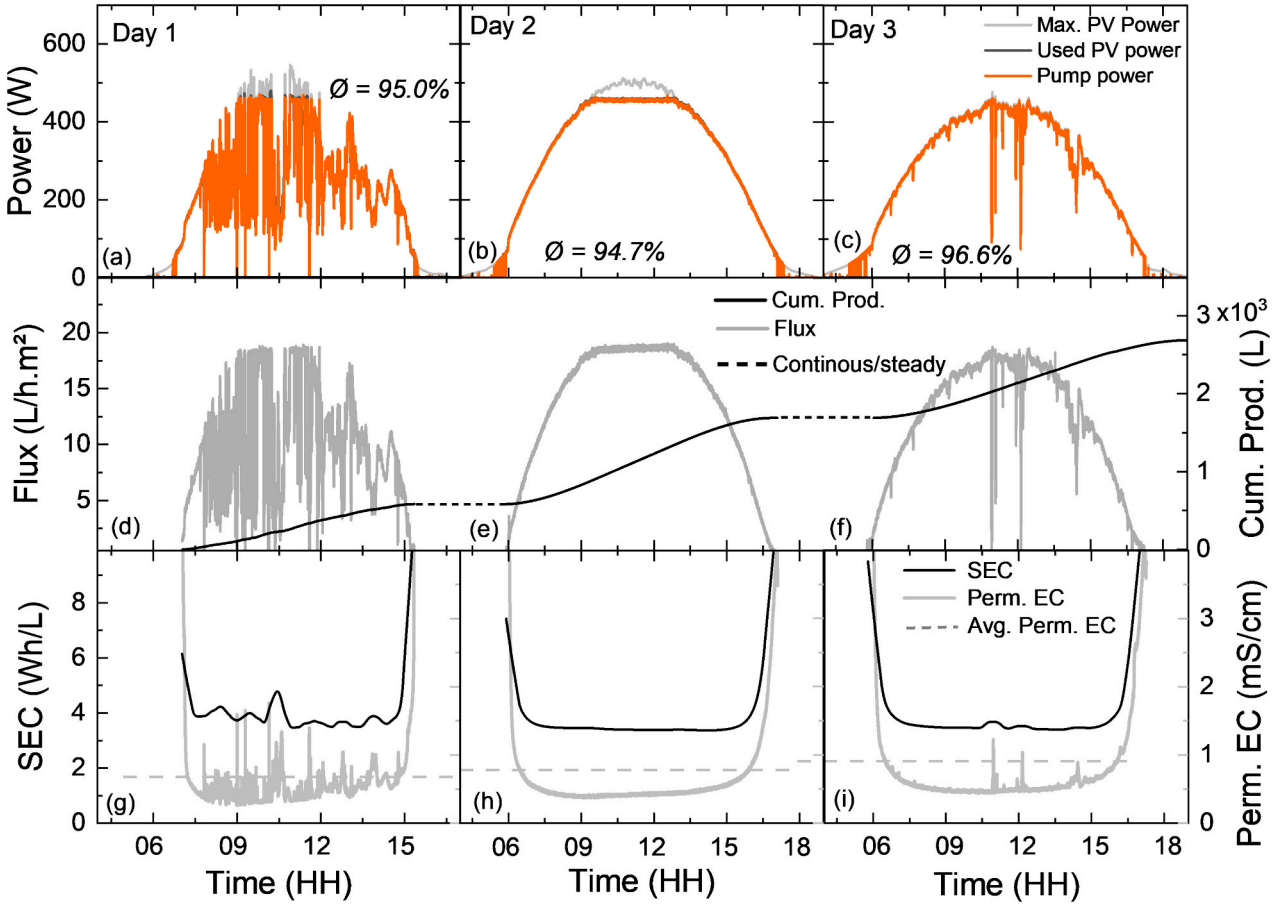

Fig. 6. System performance of a directly-coupled PV-membrane test on different solar days. For days 1–3 respectively, **(a-c)** PV power supply and usage, with Ø denoting the percentage load-matching; **(d-f)** permeate flux and cumulative daily clean water production; **(g-i)** SEC and permeate EC.

integrated for buffering the SI fluctuations and augmenting the periods of intermittencies. On day 1 (Fig. 7a), the system started off operating in directly-coupled mode until the SC discharge was initiated at 350 W following the steady-state threshold conditions in Section 3.1. However, since this method lacked the capability to recharge the storage system following each day's utilisation the SC charge became depleted after the first day. As a result, the system functioned as a directly-coupled setup for the remaining two tested days (Figs. 7b & c). The maximum load matching of 96.6% during these days was realised on a partly cloudy day (Fig. 7c).

The corresponding flux on these days resulted in the cumulative production of 2926 L (Fig. 7d-f). The SC cuts off when the charge level reaches 46 V (at approximately 30% SoC) (Fig. 7g), or when the PV power drops below P_{Pvmin} (250 W) towards the close of the day. This configuration represents an enhancement over a directly-coupled setup yielding an average permeate EC of 0.52 mS/cm and average SEC of 3.8 Wh/L (Figs. 7h-j). Due to its inability to consistently buffer subsequent day's fluctuations, the system however remained vulnerable to shut-downs during partly cloudy or overcast conditions.

3.4. Semi-active topology with PCMS (adaptive topology) – Solar days

This system comprises a semi-active configuration integrating a PCMS, designed to enable the SC to ensure sustained operational continuity while augmenting the system's overall performance by enabling a steady pump operation across the three days (see Fig. 8a-c). A maximum load matching measuring up to 99.6% was realised on these days. The corresponding flux in Fig. 8d-f resulted in cumulative production of 2758 L. Within this setup, the system enables effective utilisation of daily PV power, dynamically recharging the SC to prepare for subsequent day-long operation as shown in Fig. 8g-i. The findings from this investigation, outline the adaptability of the SC to consistently buffer different solar days, irrespective of the prevailing SI conditions. Hence, this setup is referred to as "adaptive topology".

The SC was synchronously recharged using the unutilised PV power during the off-peak period of SI. Over the three days, this system as shown in Fig. 8j-l enabled a steady operation realising an average permeate EC of 0.4 mS/cm and average SEC of 3.35 Wh/L.

3.5. Semi-active topology with PCMS (extended operation) – Solar days

To evaluate the adaptability of this configuration, the investigation

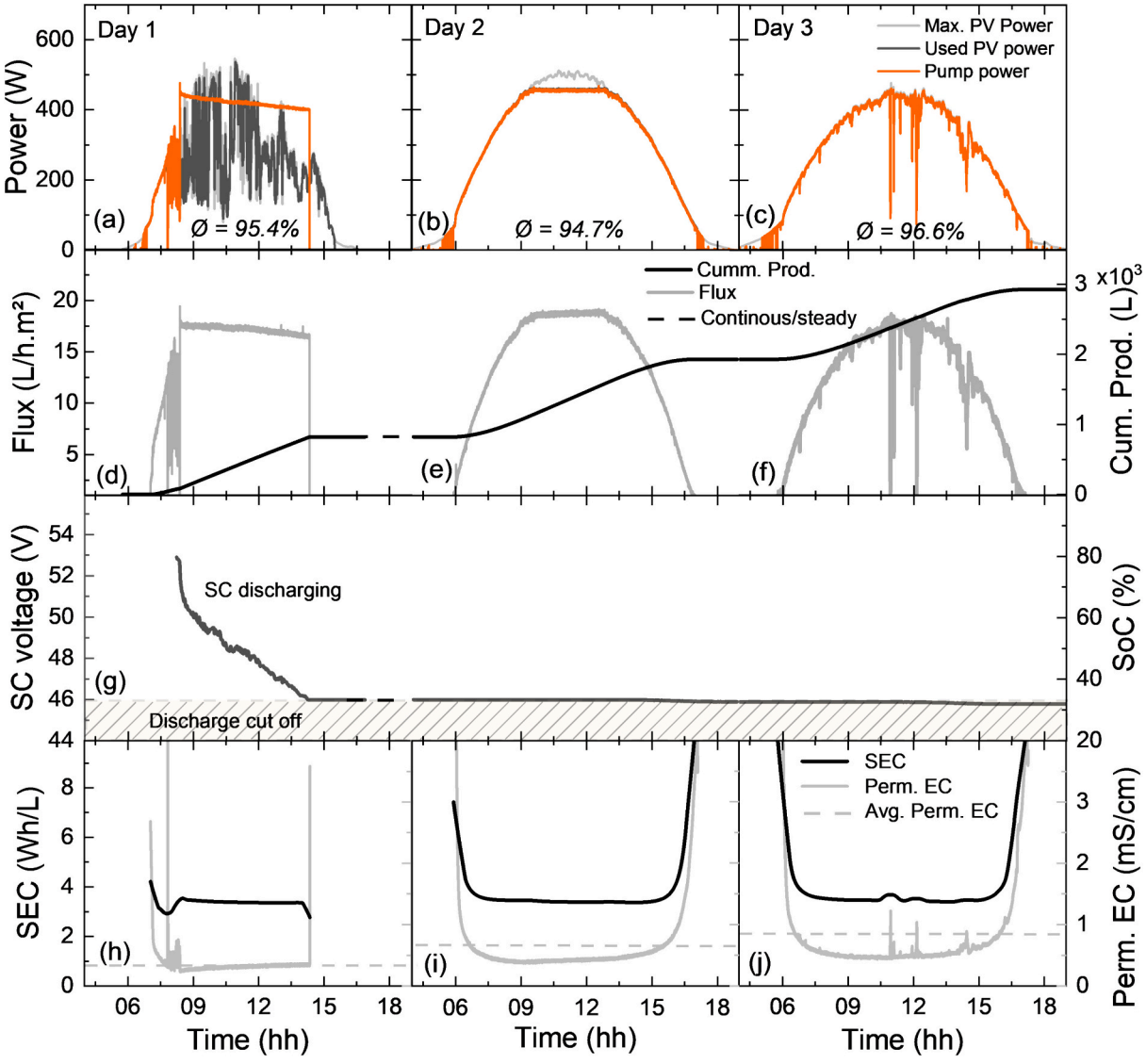

Fig. 7. System performance of a PV-membrane system with uncontrolled SC buffering. For days 1–3 respectively, **(a-c)** = PV power supply and usage, with Ø denoting the percentage load-matching; **(d-f)** = production; **g** = SC charge level; **(h-j)** = SEC and permeate EC.

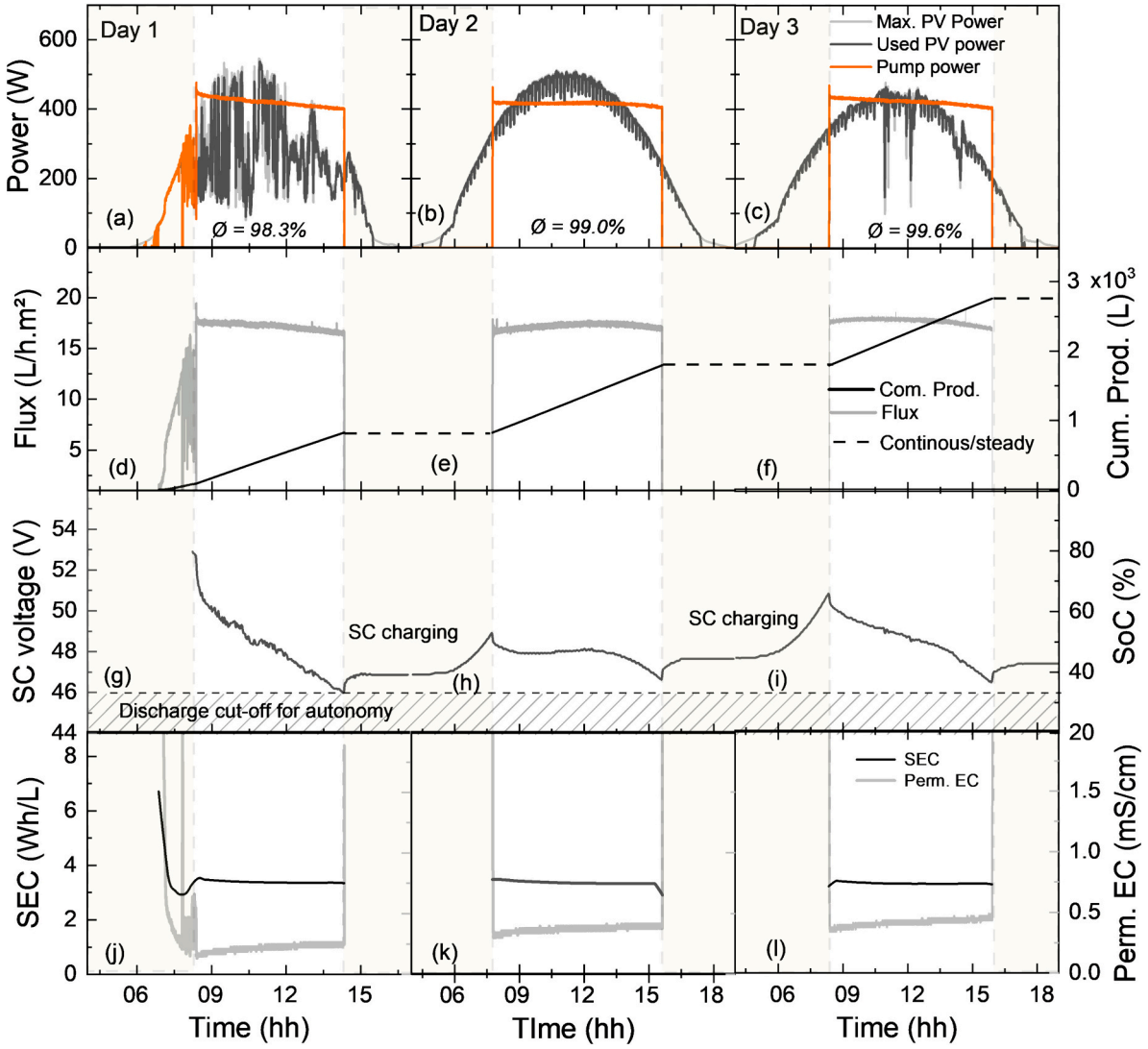

Fig. 8. PV-membrane daily system performance with controlled semi-active topology with PCMS. For days 1–3 respectively, **(a-c)** = PV power supply and usage with Ø denoting the percentage load-matching; **(d-f)** = production; **(g-i)** = SC charge level; **(j-l)** = SEC and permeate EC.

was extended into a continuous 7-day operational period, encompassing two additional days with mostly sunny conditions (days 4 & 6), one very cloudy day (day 5), and one sunny day (day 7). The additional chosen solar days were previously described in section 2.1.7. The results are depicted in Fig. 9. The steady performance of these days follows similarly as the description of the first three days. Fig. 9a-d highlight the steady operation of the pump amidst changing SI conditions across the 4 solar days. A maximum load-matching of up to 99.4% was realised during these days. Across these days, the daily flux resulted in the cumulative production of 3460 L as shown in Fig. 9e-h.

Throughout the continuous 7-day operation, the system's adaptability was assessed based on its capacity to consistently maintain the SoC of the SC to an appreciable level for subsequent day's operations (Figs. 9 **i-l**). Across this week-long period, a total production of 6218 L was achieved at an average permeate EC of 0.52 mS/cm. Furthermore, due to the system's operation at a high recovery rate, a notably low SEC was realised (Fig. 9 **m-p**) with an average of 3.32 Wh/L recorded over the 7-day duration. The overall system performance of the Investigated topologies is summarised in Table 1. It can be seen that over the 3-day period, the semi-active topology (with PCMS) afforded significant improvements in water quality, with the average permeate EC decreasing from 732 mS/cm in the directly-coupled scenario to 515 mS/cm (42% lower) and 399 mS/cm (83% lower) in the two semi-active cases (with and without PCMS), respectively. Likewise, the average SEC decreased from 4.07 kWh/m^3 (directly-coupled) to 3.83 kWh/m^3 (6% lower with semi-active without PCMS) to 3.35 kWh/m^3 (18% lower via semi-active with PCMS). The addition of SCs improves the quantity of permeate produced compared to the directly-coupled case (2926 L vs. 2687 L), however the addition of the PCMS reduces this again slightly to 2758 L. This is caused by the added inefficiency of the power electronics in the PCMS, which on very cloudy days boost the performance, but cannot provide any gain on a sunny day.

3.6. Temporal trend analysis

The temporal trend analysis of the PV membrane system with PCMS is considered over a period of 30 min on a very cloudy day between 10:30 and 11:00, as shown in Figs. 10 and 11. This challenging day (as earlier reported in section 2.1.7) is selected to investigate the temporal trends and variations in system performance due to the high levels of SI fluctuations. This day was evaluated using a directly-coupled topology and a semi-active topology with the integrated PCMS.

In the directly-coupled (passive) system, rapid fluctuations in PV power supply, attributed to SI fluctuations, lead to similar fluctuations in pump operation (Fig. 10a), given the absence of SC energy buffering (Fig. 10b). The resulting flux production exhibits a comparable

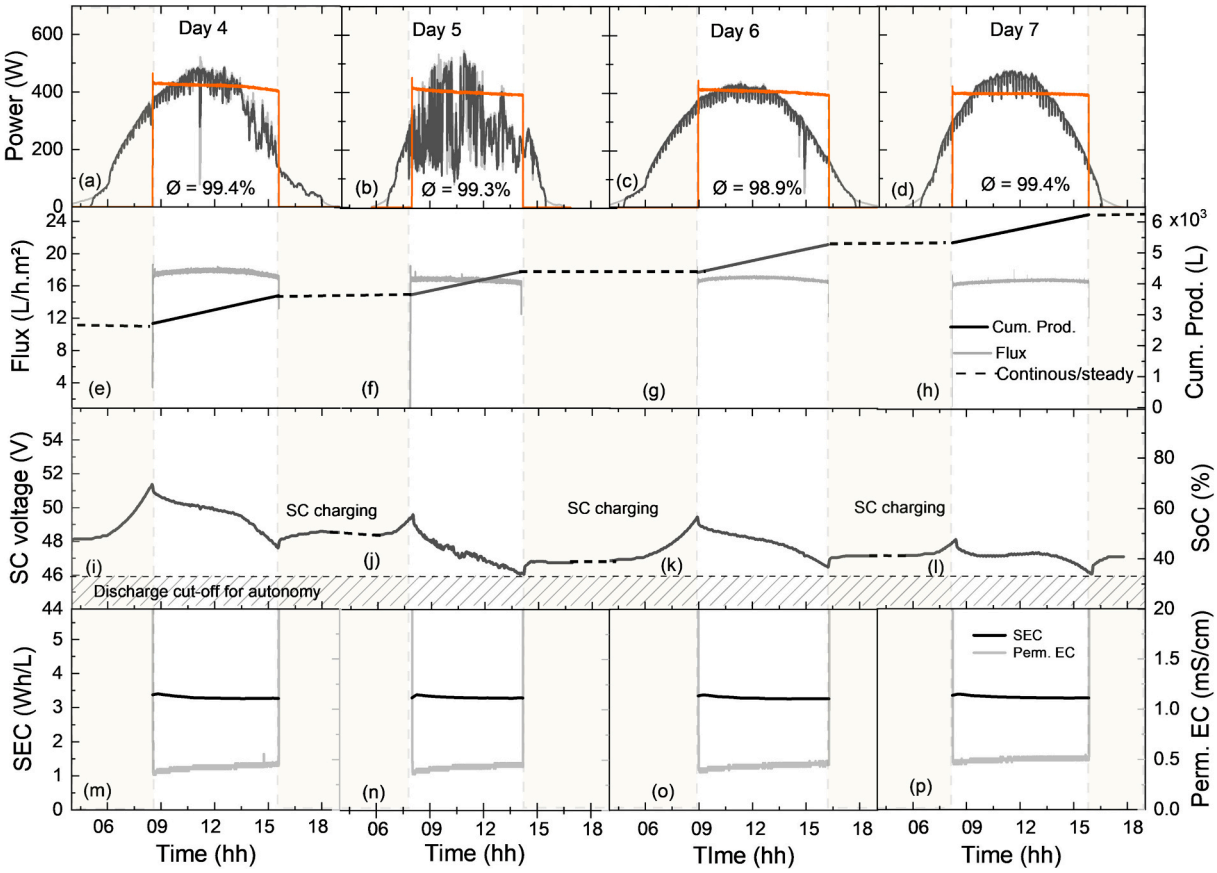

Fig. 9. PV-membrane daily system performance with controlled semi-active topology. For days 4–7 respectively, **(a-d)** = PV power supply and usage with Ø denoting the percentage load-matching; **(e-h)** = production, **(i-l)** = SC charge level, **(m-p)** = SEC and permeate EC.

Table 1
System performance of the investigated topologies.

Investigated topologies	Day	System performance									
		Max. PV energy (Wh)	Used PV energy (Wh)	Pump energy (Wh)	Load match factor Ø (%)	SC round-trip energy (Wh)	Daily Prod. (L)	Cum Prod. (L)	Avg. daily SEC (Wh/L)	Avg.daily. Perm. EC (mS/cm)	Avg. perm. C (mS/cm)
Passive topology	1	2252	2140	2140	95.0	N/A	582	2687	4.10	0.61	732
	2	4094	3875	3875	94.7	N/A	1108		4.00	0.71	
	3	3692	3568	3568	96.6	N/A	997		4.10	0.87	
Semi-active (without PCMS)	1	2252	2148	2779	95.4	762	821		3.40	0.37	
	2	4094	3875	3875	94.7	N/A	1108	2926	4.00	0.71	515
	3	3692	3568	3568	96.6	N/A	997		4.10	0.87	
Semi-active (with PCMS)	1	2252	2214	2779	98.3	760	823		3.42	0.37	
	2	4094	4055	3264	99.0	−256	970	2758	3.35	0.39	399
	3	3692	3678	3181	99.6	−26	965		3.29	0.44	
Extended operation: Semi-active with PCMS	4	3624	3602	2969	99.4	−173	900		3.29	0.45	
	5	2252	2235	2490	99.3	519	750	3460	3.31	0.46	636
	6	3664	3625	2969	98.9	−181	900		3.27	0.49	
	7	3314	3293	3012	99.4	−275	910		3.29	0.52	

fluctuation pattern (Fig. 10c). Notably, during ramp-down events in PV power supply, there is a corresponding increase in permeate EC, indicative of reduced water quality, while SEC gradually diminishes as the PV power supply increases (Fig. 10d).

Conversely, the semi-active topology with integrated PCMS demonstrates consistent pump operation (Fig. 11a), owing to the buffering support provided by the SC (Fig. 11b). The SC undergoes charging when the power supply exceeds the demand threshold. Compared to the passive system, this configuration yields steady and enhanced flux production (Fig. 11c), along with reduced SEC and EC values, indicating improved water quality (Fig. 11d). It is also worth noting that, following the control algorithm (Fig. 4), the SC can also significantly charge during the negative deviation periods when the pump is not running.

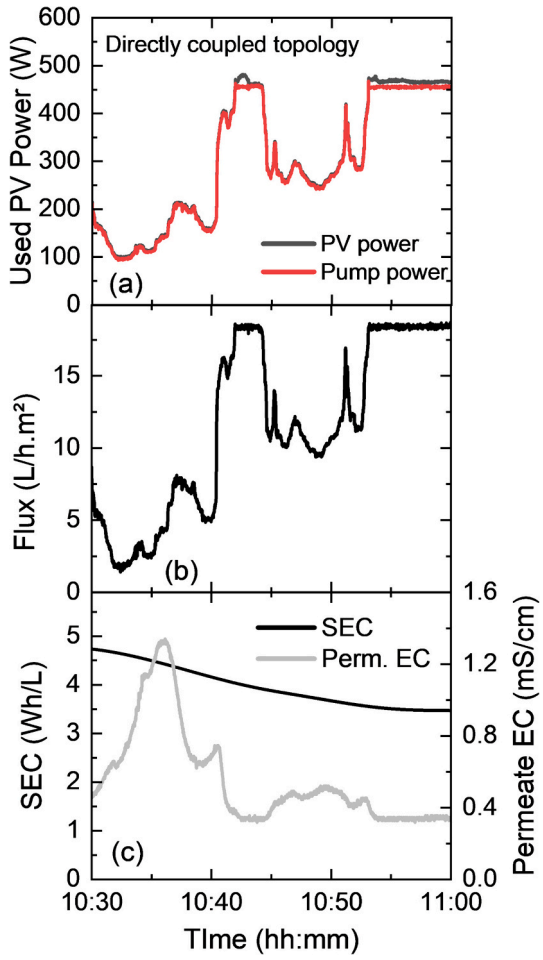

Fig. 10. Temporal trend analysis of PV-membrane system when operated in a directly-coupled (passive) topology. (a) PV power supply and power consumed by the pump; (b) Fluctuating flux through the membrane due to changing PV power supply; (c) SEC and permeate EC.

3.7. Further discussion and feasibility outlook

The SC roundtrip energy in Table 1. signifies the net energy variation resulting from the daily charging and discharging procedures of the SC. In this context, the negative notation denotes the net energy gained, while the positive notation indicates the net energy delivered. This notation is to align the sign conventions applied to other energy measurements within the system to maintain consistency across energy value representations. The SC's roundtrip energy in this context does not precisely equate to the difference between the used PV energy and the pump's energy. Instead, it hinges on the SC's capacity to provide support and buffering during periods of both low and fluctuating PV power supply, and this can be influenced by potential power loss attributable to switching losses and the efficiency of the charge controller during these operational phases. These factors will be the subject of further investigation to precisely ascertain the total energy dynamics associated with the SC's role in the system.

Additionally, due to the linear discharge characteristics of SCs, the SC voltage decreases steadily during discharge. In scenarios necessitating a sustained current output as in this work, the total SC power output thus exhibited a gradual decline as the discharge process continued. This effect was notable across the investigated topologies where SC energy support was incorporated. The gradual decline in the SC power resulted in the delivered flux following a similar trend which resulted in a gradual upward trend in the daily permeate EC such as the shown in Fig. 9m-p.

Meanwhile the results from the implementation of the PCMS demonstrate enhancements in permeate quality and SEC. To determine the potential long-term impacts of the improvements, the projected year-long production per topology (passive and semi-active with PCMS was estimated using a year-long SI data of KIT Solar Park (2016). Based on the STCs of the PV panels utilised in this study (as outlined in section 2.1.1), a peak SI of 1000 W/m^2 corresponds to approximately 600 W_p of the PV panels. This implies an approximate PV power generation of 0.6 W_p per W/m^2 of SI. The daily SI was multiplied by this ratio to determine the instantaneous PV power generated per second, which was then converted to energy units (Wh) by dividing each power value by a factor of 3600. Subsequently, the PV energy was divided by the average SEC (Wh/L) of the topologies and integrated over a year comprising 366 days. The average SEC over three days was used to give a more accurate representation of each topology's performance during sustained operation. As outlined in Table S3 and Fig. S4 of the supplementary information, the outcomes reveal a potential annual production increase of approximately 39,416 L with the adoption of the adaptive topology with PCMS, compared to the passive topology setup.

The practical feasibility of implementing a PV-membrane system as previously reported in other studies [11,37,67,69,70] indicate that, firstly, this technology offers far greater sustainability for long-term usage (up to 20 years) [67]. Secondly, the decentralized and modular nature of the PV-membrane system makes it readily deployable in remote areas of both developed and developing countries – all that is needed is a contaminated water source. Such systems obviously contribute directly to the UN SDGs 6 (clean water) and 7 (clean energy), however – and perhaps more importantly – there are also indirect and longer-term contributions to SDG 3 (good health, promoted by the lack of water-borne diseases), SDG 5 (gender equality, since it is typically women who have the role of collecting water [70]), and SDG 4 (quality education, since children who would need to walk long distances to collect water now have a better chance of attending school) [69,70]. It is also worth noting that our system is the most recent in a development of prototypes developed over the past two decades, which have been tested in locations such as outback Australia [71], and northern Tanzania [11], both powered by PV, as well as a wind-energy-powered version in Scotland [37].

Thirdly, the PV-membrane system is particularly advantageous given that the solar power being produced from the PV panels is currently guaranteed for up to 40 years [67,72,73]. Moreover, solar PV energy stands out as one of the most cost-effective energy sources, with an average global levelized cost of electricity (LCOE) at about 0.05 $/kWh [74], while the average LCOE in Africa is in the range of 0.031–0.093 $/kWh [75].

Fourthly, the levelized cost of water (LCOW) provided by a PV-membrane system has been observed to be typically below the water cost in developing countries [76]. For instance, the estimated water cost for desalination of brackish water with PV-membrane system could fall within 0.82–1.34 $/m^3 [70] while the cost of water supply in remote communities in Sub-Saharan Africa has been reported higher, for example 1.3 to 4.5 $/m^3 in Ghana [77] and about 1.32 $/m^3 in Tanzania [78].

With the PCMS in this study, a relatively low SEC of approximately 3.3 Wh/L per day was realised during an extended operation of one week. Moreover, the SC module utilised in this study boasts a lifespan capable of enduring up to 1 million cycles, while the PLC can sustain prolonged years of operation with right maintenance of the hardware and regular update of the software [79–82]. The extended lifespan of the integrated components and low SEC underscore the practical feasibility of the system for implementation, aiming for a projected operational lifespan of 20 years."

4. Conclusions

This study presents an empirical investigation of three DC coupling

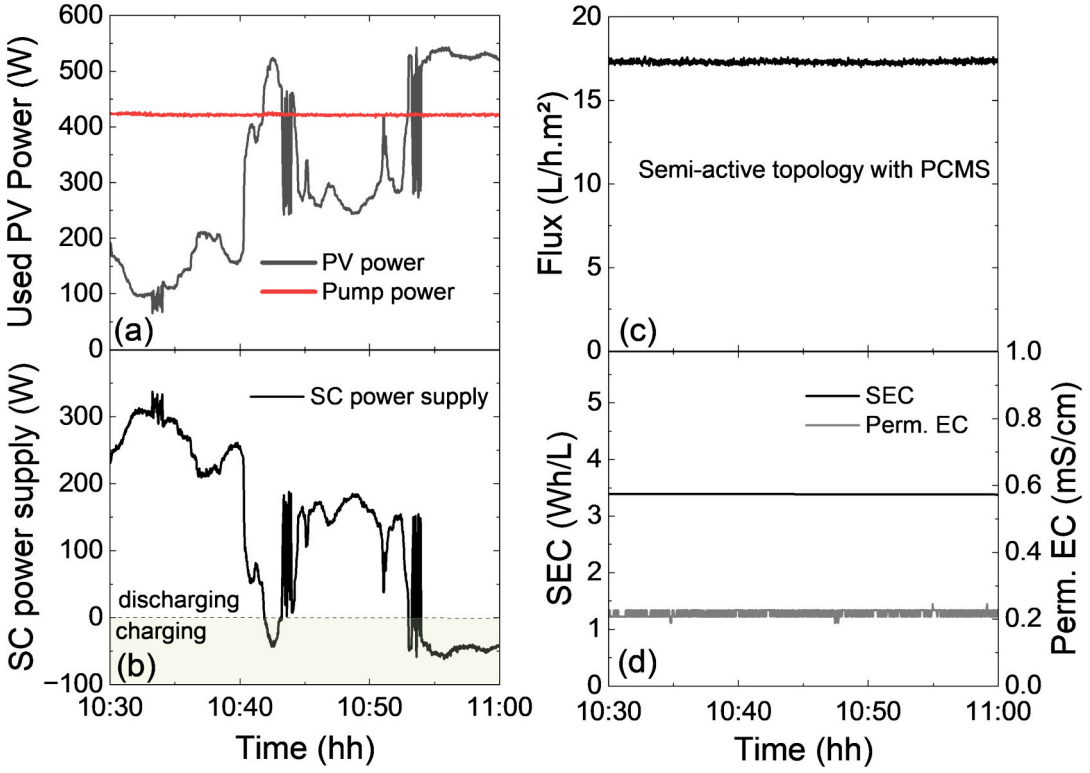

Fig. 11. Temporal trend analysis of PV-membrane system with using semi-active topology with integrated PCMS. (a) PV power supply and power consumed by the pump; (b) Power supply by the SC showing the charging and discharging state with reference to the changing SI level; (c) Steady flux through the membrane due to steady pump power; (d) SEC and permeate EC.

topologies aimed at maximising the utilisation of daily PV energy for sustaining an autonomous PV-membrane filtration system across multiple solar days under different SI conditions. These topologies are directly-coupled without SC (passive topology), a modified semi-active topology (without PCMS) and a controlled semi-active topology with an integrated PCMS (adaptive topology).

The results show that the passive system, as mostly employed in PV-membrane setups, is susceptible to SI fluctuations. This occasionally resulted in increased SEC, reduced permeate quality, and frequent system shutdowns. The semi-active topology (without PCMS) commonly utilised in buffering scenarios, however, lacked the capacity to recharge the storage unit post daily operation. Consequently, the system is prompt to always revert to passive topology on the depletion of the SC's charge after the first day of operation. The proposed adaptive topology facilitated the recharging of the SC during each day's operation ensuring sustained system performance (SEC, permeate EC, production) under varying SI conditions, thus enabling the system's adaptability to varying solar days.

Across a three-day investigation, the proposed adaptive topology integrating the PCMS exhibited an average permeate EC of 0.40 mS/cm, marking a 46% improvement over the directly-coupled topology and a 23% enhancement compared to the uncontrolled semi-active topology. The adaptive topology also enabled an average SEC of 3.35 Wh/L, while the average daily SEC for the directly-coupled and uncontrolled semi-active systems was realised at 4.1 and 3.8 Wh/L respectively.

During a one-week extended operation of the controlled topology, the system achieved a cumulative production of 6218 L at an average permeate quality of 0.52 Wh/L, while the SoC of the supercapacitor was maintained within the 40% range. Additionally, this proposed adaptive topology demonstrated superior load-matching efficiency, reaching up to 99.6% compared to the highest value of 96.6% observed in both passive and uncontrolled semi-active topology-based systems.

CRediT authorship contribution statement

Emmanuel Ogunniyi: Writing – original draft, Validation, Software, Methodology, Investigation, Formal analysis, Conceptualization. **Bryce S. Richards:** Writing – review & editing, Visualization, Supervision, Resources, Project administration, Methodology, Funding acquisition, Formal analysis, Conceptualization.

Declaration of competing interest

The authors declare that they have no known competing financial interests or personal relationships that could have appeared to influence the work reported in this paper.

Data availability

Data will be made available on request.

Acknowledgements

The authors would like to acknowledge: the PhD scholarship for Emmanuel Ogunniyi provided by the Deutscher Akademischer Austauschdienst (DAAD) Research Grant for Doctoral Programmes in Germany; Achim Voigt (KIT) for providing valuable support and guidance regarding electronic devices acquisition, installation and ensuring equipment compliance with regulatory standards; Jürgen Benz (KIT) for assisting with laboratory set up and ensuring safety; Dr. Dmitry Busko (KIT) for insightful contributions towards the system setup; and Dr. Youssef-Amine Boussouga (KIT) for trouble-shooting. Bryce Richards gratefully acknowledges funding from The Helmholtz Association via the Materials and Technologies for the Energy Transition (MTET) program – Topic 1 – Photovoltaics (38.01.04), and the professorial recruitment initiative.

Appendix A. Supplementary data

Supplementary data to this article can be found online at https://doi.org/10.1016/j.apenergy.2024.123624.

References

[1] DeNicola E, Aburizaiza OS, Siddique A, Khwaja H, Carpenter DO. Climate change and water scarcity: the case of Saudi Arabia. Ann Glob Health 2015;81(3):342–53.
[2] Gleick PH, Cooley H. Freshwater scarcity. Annu Rev Environ Resour 2021;46:319–48.
[3] Ueda S, Kawabata H, Hasegawa H, Kondo K. Characteristics of fluctuations in salinity and water quality in brackish Lake Obuchi. Limnology 2000;1:57–62.
[4] Gray SR, Semiat R, Duke M, Rahardianto A, Cohen Y. Seawater use and desalination technology. 2011.
[5] Connor R. The United Nations world water development report 2015: water for a sustainable world, 1. UNESCO publishing; 2015. p. 37–41.
[6] Lapworth D, et al. Drinking water quality from rural handpump-boreholes in Africa. Environ Res Lett 2020;15(6):064020.
[7] EPA. "Secondary Drinking Water Standards: Guidance for Nuisance Chemicals," United States Enviromental Protection Agency. Accessed: 02.02 [Online]. Available, https://www.epa.gov/sdwa/secondary-drinking-water-standards-guidance-nuisance-chemicals; 2024.
[8] Ram A, Tiwari S, Pandey H, Chaurasia AK, Singh S, Singh Y. Groundwater quality assessment using water quality index (WQI) under GIS framework. Appl Water Sci 2021;11:1–20.
[9] World Health Organization(WHO). Guidelines for drinking-water quality: Incorporating the first and second addenda. World Health Organization; 2022.
[10] Nassrullah H, Anis SF, Hashaikeh R, Hilal N. Energy for desalination: a state-of-the-art review. Desalination 2020;491:114569.
[11] Schäfer AI, Shen J, Richards BS. "Renewable energy-powered membrane technology in Tanzanian communities," *npj clean*. Water 2018;1(1):24.
[12] Applebaum J. The quality of load matching in a direct-coupling photovoltaic system. IEEE Transact on Energy Conv 1987;4:534–41.
[13] Khatib T, Muhsen D. "Photovoltaic water pumping systems concept," in *Photovoltaic Water Pumping Systems: Concept, Design, and Methods of Optimization*: Academic Press. 2020. ch. 2.
[14] Richards BS, Capão DP, Früh WG, Schäfer AI. Renewable energy powered membrane technology: impact of solar irradiance fluctuations on performance of a brackish water reverse osmosis system. Sep Purif Technol 2015;156:379–90.
[15] Li S, de Carvalho AP, Schäfer AI, Richards BS. Renewable energy powered membrane technology: electrical energy storage options for a photovoltaic-powered brackish water desalination system. Appl Sci 2021;11(2):856.
[16] Freire-Gormaly M, Bilton A. Experimental quantification of the effect of intermittent operation on membrane performance of solar powered reverse osmosis desalination systems. Desalination 2018;435:188–97.
[17] Li S, Voigt A, Schäfer AI, Richards BS. Renewable energy powered membrane technology: energy buffering control system for improved resilience to periodic fluctuations of solar irradiance. Renew Energy 2020;149:877–89.
[18] Turki M, Belhadj J, Roboam X. Real time energy-Water management fulfilling integrity constraints of a reverse osmosis desalination system powered by a renewable source. Available at SSRN 2023;4326457.
[19] Khouzam KY. Optimum load matching in direct-coupled photovoltaic power systems-application to resistive loads. IEEE Transact on Energy Conv 1990;5(2):265–71.
[20] Balouktsis A, Karapantsios T, Anastasiou K, Antoniadis A, Balouktsis I. Load matching in a direct-coupled photovoltaic system-application to Thevenin's equivalent loads. Int J Photoenergy 2006;2006.
[21] Groumpos P, Papegeorgiou G. An optimum load management strategy for stand-alone photovoltaic power systems. Sol Energy 1991;46(2):121–8.
[22] Tan K, Parquette WJ, Tao M. A predictive algorithm for maximum power point tracking in solar photovoltaic systems through load management. Sol Energy 2023;265:112127.
[23] Nelik L. Centrifugal & rotary pumps: Fundamentals with applications. CRC press; 1999.
[24] Volk M. Pump characteristics and applications. CRC Press; 2013.
[25] Gevorkov L, Domínguez-García JL, Romero LT. Review on solar photovoltaic-powered pumping systems. Energies 2022;16(1):94.
[26] Vodovozov V, Lehtla T, Bakman I, Raud Z, Gevorkov L. "Energy-efficient predictive control of centrifugal multi-pump stations," in *2016 Electric Power Quality and Supply Reliability (PQ)*. 2016. IEEE, pp. 233–238.
[27] Khouzam KY. The load matching approach to sizing photovoltaic systems with short-term energy storage. Sol Energy 1994;53(5):403–9.
[28] Khatib T. Deign of photovoltaic water pumping systems at minimum. J Appl Sci 2010;10:2773–84.
[29] Kolhe M, Joshi J, Kothari D. Performance analysis of a directly coupled photovoltaic water-pumping system. IEEE Transact on Energy Conv 2004;19(3):613–8.
[30] Mahmoud MM, Kukhun WR, Daud A-K. Efficiency improvement of a dual PV water pumping system on a desert well by solar matched load control. Intern J Energ Engineering 2013;3(5):151.
[31] Akbaba M. Optimum matching parameters of an MPPT unit used for a PVG-powered water pumping system for maximum power transfer. Int J Energy Res 2006;30(6):395–409.
[32] Ghenai C, Bettayeb M. Design and optimization of grid-tied and off-grid solar PV systems for super-efficient electrical appliances. Energ Effic 2020;13:291–305.
[33] Obaro AZ, Munda JL, Yusuff AA. Modelling and energy Management of an off-Grid Distributed Energy System: a typical community scenario in South Africa. Energies 2023;16(2):693.
[34] Shahid MK, et al. A review of membrane-based desalination systems powered by renewable energy sources. Water 2023;15(3):534.
[35] Zein A, Karaki S, Al-Hindi M. Analysis of variable reverse osmosis operation powered by solar energy. Renew Energy 2023;208:385–98.
[36] Tigrine Z, et al. Feasibility study of a reverse osmosis desalination unit powered by photovoltaic panels for a sustainable Water supply in Algeria. Sustainability 2023;15(19):14189.
[37] Richards BS, Park GL, Pietzsch T, Schäfer AI. Renewable energy powered membrane technology: brackish water desalination system operated using real wind fluctuations and energy buffering. J Membr Sci 2014;468:224–32.
[38] Shen J, Jeihanipour A, Richards BS, Schäfer AI. Renewable energy powered membrane technology: experimental investigation of system performance with variable module size and fluctuating energy. Sep Purif Technol 2019;221:64–73.
[39] DupontFilmTec. "Reverse Osmosis Membranes Technical Manual," in "Dupont Water Solutions." Available. https://www.dupont.com/content/dam/dupont/amer/us/en/water-solutions/public/documents/en/RO-NF-FilmTec-Manual-45-D01504-en.pdf; 2024. Accessed on: 02.02.
[40] McCormick P, Suehrcke H. The effect of intermittent solar radiation on the performance of PV systems. Sol Energy 2018;171:667–74.
[41] Schnabel J, Valkealahti S. Energy storage requirements for PV power ramp rate control in northern Europe. Int J Photoenergy 2016;2016.
[42] Shivashankar S, Mekhilef S, Mokhlis H, Karimi M. Mitigating methods of power fluctuation of photovoltaic (PV) sources–a review. Renew Sust Energ Rev 2016;59:1170–84.
[43] Jossen A, Garche J, Sauer DU. Operation conditions of batteries in PV applications. Sol Energy 2004;76(6):759–69.
[44] Hajiaghasi S, Salemnia A, Hamzeh M. Hybrid energy storage system for microgrids applications: a review. J Energ Storage 2019;21:543–70.
[45] Ogunniyi E, Pienaar H. "Overview of battery energy storage system advancement for renewable (photovoltaic) energy applications," in *2017 International Conference on the Domestic Use of Energy (DUE)*. 2017. IEEE, pp. 233–239.
[46] Jaszczur M, Hassan Q. An optimisation and sizing of photovoltaic system with supercapacitor for improving self-consumption. Appl Energy 2020;279:115776.
[47] Du Pasquier A, Plitz I, Menocal S, Amatucci G. A comparative study of Li-ion battery, supercapacitor and nonaqueous asymmetric hybrid devices for automotive applications. J Power Sources 2003;115(1):171–8.
[48] Xu H, Shen M. The control of lithium-ion batteries and supercapacitors in hybrid energy storage systems for electric vehicles: a review. Int J Energy Res 2021;45(15):20524–44.
[49] Song Z, Hofmann H, Li J, Han X, Zhang X, Ouyang M. A comparison study of different semi-active hybrid energy storage system topologies for electric vehicles. J Power Sources 2015;274:400–11.
[50] Bhattacharyya P, Banerjee A, Sen S, Giri SK, Sadhukhan S. "A Modified Semi-Active Topology for Battery-Ultracapacitor Hybrid Energy Storage System for EV Applications," in *2020 IEEE International Conference on Power Electronics, Smart Grid and Renewable Energy (PESGRE2020)*. 2020. IEEE, pp. 1–6.
[51] Ibanez FM, Florez AMB, Gutiérrez S, Echeverría JM. Extending the autonomy of a battery for electric motorcycles. IEEE Trans Veh Technol 2019;68(4):3294–305.
[52] Min H, Lai C, Yu Y, Zhu T, Zhang C. Comparison study of two semi-active hybrid energy storage systems for hybrid electric vehicle applications and their experimental validation. Energies 2017;10(3):279.
[53] Glavin M, Chan PK, Armstrong S, Hurley W. "a stand-alone photovoltaic supercapacitor battery hybrid energy storage system," in *2008 13th international power electronics and motion control conference*, 2008: IEEE, pp. 1688-1695.
[54] Jing W, Lai CH, Wong WS, Wong MD. A comprehensive study of battery-supercapacitor hybrid energy storage system for standalone PV power system in rural electrification. Appl Energy 2018;224:340–56.
[55] Xiong R, Chen H, Wang C, Sun F. Towards a smarter hybrid energy storage system based on battery and ultracapacitor-a critical review on topology and energy management. J Clean Prod 2018;202:1228–40.
[56] Zeraati M, Golshan MEH, Guerrero JM. Distributed control of battery energy storage systems for voltage regulation in distribution networks with high PV penetration. IEEE Transactions on Smart Grid 2016;9(4):3582–93.
[57] Zuo W, Li R, Zhou C, Li Y, Xia J, Liu J. Battery-supercapacitor hybrid devices: recent progress and future prospects. Adv sci 2017;4(7):1600539.
[58] Maleki A. Design and optimization of autonomous solar-wind-reverse osmosis desalination systems coupling battery and hydrogen energy storage by an improved bee algorithm. Desalination 2018;435:221–34.
[59] Chen W, Li Y, Liu Z, Hong Y. Understanding of energy conversion and losses in a centrifugal pump impeller. Energy 2023;263:125787.
[60] Habib S, et al. Technical modelling of solar photovoltaic water pumping system and evaluation of system performance and their socio-economic impact. Heliyon 2023;9(5).
[61] Karunanithi K, Ramesh S, Raja S, Sreedhar R, Kannan S, Ramudu V. Investigations of standalone PV system with battery-supercapacitor hybrid energy storage system for household applications. Int J Inf Technol 2023;15(1):279–87.
[62] Sohrabi A, Meratizaman M, Liu S. Comparative analysis of integrating standalone renewable energy sources with brackish water reverse osmosis plants: technical and economic perspectives. Desalination 2024;571:117106.
[63] Eghtedarpour N, Farjah E. Power control and management in a hybrid AC/DC microgrid. IEEE transactions on smart grid 2014;5(3):1494–505.

[64] Zhou T, François B. Energy management and power control of a hybrid active wind generator for distributed power generation and grid integration. IEEE Trans Ind Electron 2010;58(1):95–104.
[65] Shiau J-K, Ma D-M, Yang P-Y, Wang G-F, Gong JH. Design of a solar power management system for an experimental UAV. IEEE Trans Aerosp Electron Syst 2009;45(4):1350–60.
[66] ChromaUSA. "Programmable DC Power Supply." Accessed [Online]. Available, https://www.chromausa.com/product/dc-power-supply-62000h/; 01.04.2024.
[67] Li S, Cai Y-H, Schäfer AI, Richards BS. Renewable energy powered membrane technology: a review of the reliability of photovoltaic-powered membrane system components for brackish water desalination. Appl Energy 2019;253:113524.
[68] Grundfos. SQF 0.6–2 N. Available, https://product-selection.grundfos.com/products/sqflex/sqf-06-2-n-95027325?pumpsystemid=2328476622&tab=variant-curves; 02.02.2024. Accessed on.
[69] Desa U. Transforming our world: The 2030 agenda for sustainable development. 2016.
[70] Water U. Summary Progress update 2021: SDG 6—Water and sanitation for all. Geneva: Switzerland; 2021.
[71] Richards BS, Capão DPS, Schäfer AI. Renewable energy powered membrane technology. 2. The effect of energy fluctuations on performance of a photovoltaic hybrid membrane system. Environ Sci Technol 2008;42(12):4563–9.
[72] Villessot D, Vergnet M, Garel T, Vallon D, Chesneau J. "drinking water production by solar reverse osmosis: Returns and performances from field operation," *TSM. Genie Urbain Genie Rural: Techniques Sciences Methodes*; 2019. p. 27–38.
[73] SunPower. SunPower Maxeon Panel 40-Year Warranty. Available, https://sunpower.maxeon.com/int/solar-panel-products/warranty; 2024. Accessed on: 19.04.2024.
[74] IRENA. Renewable Power Generation Cost 2022. Available, https://www.irena.org/Publications/2023/Aug/Renewable-Power-Generation-Costs-in-2022#:~:text=For%20newly%20commissioned%20onshore%20wind,2022%20to%20USD%200.049%2FkWh,2022%20to%20USD%200.049%2FkWh; 2022. Accessed on: 04.04.2024.
[75] IEA. "International Energy Agency. Levelized cost of electricity by technology in Africa in the Sustainable Africa Scenario 2022–2030," in "Africa Energy Outlook 2022,". Available, https://www.iea.org/data-and-statistics/charts/levelised-cost-of-electricity-by-technology-in-africa-in-the-sustainable-africa-scenario-2020-2030; 2022. Accessed on: 04.04.2024.
[76] Schäfer AI, Hughes G, Richards BS. Renewable energy powered membrane technology: a leapfrog approach to rural water treatment in developing countries? Renew Sust Energ Rev 2014;40:542–56.
[77] G. Community Water Sanitation Agency. Groundwater Development for Small Towns Water Supply, Ghana. Available, https://www.geosearch.co.uk/water/ghana/ghana_text.htm. Accessed on: 04.04.2024.
[78] N. W. S. A. S. Authority The water supply and sanitation act. Available, https://www.ewura.go.tz/wp-content/uploads/2023/11/GN.-640-Orkesumet-WSSA-Tariff-Order-2023-English.pdf; 2023. Accessed on: 04.04.2024.
[79] Alphonsus ER, Abdullah MO. A review on the applications of programmable logic controllers (PLCs). Renew Sust Energ Rev 2016;60:1185–205.
[80] Al-Najari B. "design and implementation of control cabinet based Siemens S7–300 programmable logic controller PLC," in *proceedings of 2nd international multi-disciplinary conference theme: Integrated sciences and technologies, IMDC-IST 2021, 7–9 September 2021*. Turkey: Sakarya; 2022.
[81] Bolton W. Programmable logic controllers. Newnes; 2015.
[82] Euautomation. Extending your PLC's Lifespan. Available, https://assets.euautomation.com/automated/guides/en/PLCsLifespanEN.pdf. Accessed on: 01.04.2024.